

# Propagation of Elongated Fluid-Driven Fractures: Rock Toughness vs. Fluid Viscosity\*

Dmitry I. Garagash

February 3, 2025

Dalhousie University, Department of Civil and Resource Engineering, Halifax, Canada  
garagash@dal.ca

## Abstract

This paper studies the effect of the rock fracture toughness on the propagation of elongated fluid-driven fractures. We use the ‘tough PKN’ model of Sarvaramini and Garagash (2015), an extension of the classical PKN model (Perkins and Kern, 1961; Nordgren, 1972), which allows for a non-zero energy release rate into the advancing fracture front(s). We provide a self-consistent analysis of a ‘tough’ elongated fracture driven by arbitrary fluid injection law under assumption of the negligible fluid leak-off. We use scaling considerations to identify the non-dimensional parameters governing the propagation regimes and their succession in time, provide a number of analytical solutions in the limiting regimes for an arbitrary power-law injection, and also posit a simplified, equation-of-motion, approach to solve a general elongated fracture propagation problem during the injection and shut-in periods. Finally, we use the developed solutions for a tough elongated fracture to surmise the relative importance of the viscous and toughness-related dissipation on the fracture dynamics and broach the implications of the possible toughness scale-dependence.

## Key points:

1. Model for propagation of elongated hydraulic fractures accounting for solid toughness and fluid viscosity for varied fluid injection scenarios.
2. Analytical solutions for end-member toughness- and viscosity-dominated regimes for a power-law and exponential fluid injection in time.
3. Solution to the transient fracture growth in mixed (toughness-viscosity) regime by a numerical and a simplified analytical Equation-of-Motion approaches.

## 1 Introduction

This paper studies propagation of three-dimensional hydraulic fractures when one of its dimensions (e.g. height) remains constrained. These ‘elongated’ hydraulic fractures arise in geo-reservoirs stimulation applications (Perkins and Kern, 1961; Nordgren, 1972; Adachi et al.,

---

\*submitted for consideration for publication in ASME Journal of Applied Mechanics

2006), as well as, occur naturally, such as in the joint formation in pore-fluid-overpressured sedimentary strata (Pollard and Aydin, 1988), lateral magma emplacement in rift-zones by blade-like dikes (Rubin and Pollard, 1987; Rivalta et al., 2015), vertical magma transport in the crust by buoyant dikes with toughness constrained breadth (Garagash and Germanovich, 2014, 2022; Davis et al., 2020; Möri and Lecampion, 2022). Fig. 1a shows a conceptualized bi-wing, elongated fracture of height  $2b$  and length  $2\ell(t)$  with  $\ell \gg b$  driven by the volumetric fluid source  $2V(t)$  at the center. Fig. 1b,c show the relocated micro-seismicity recorded during propagation of an industrial hydraulic fracture in Carthage Cotton Valley Gas Field, Texas (Rutledge et al., 2004; Mayerhofer et al., 2000), highlighting the final spatial extent of an elongated fracture. Lithological layering and related stress barriers to hydraulic fracture vertical propagation are usually evoked to explain the laterally-elongated (constrained height) fracture in hydraulic fracturing in geo-energy applications (e.g., Adachi et al., 2010; Möri et al., 2024) and in formation of natural joints by pore fluid overpressure (Pollard and Aydin, 1988), while density-stratification of the crust in rifting zones and associated reversal of the magma buoyancy in shallow crust can lead to the formation and sustained lateral growth of blade-like dikes (Rubin and Pollard, 1987; Lister, 1990; Townsend et al., 2017).

## 1.1 Elongated hydraulic fracture modeling

The classical PKN (Perkins and Kern, 1961; Nordgren, 1972) model of elongated hydraulic fracturing is based on *two main assumptions*.

1. The crack length is much larger than the height, which allows to neglect elastic stress transfer along the elongated crack dimension and thus model a vertical fracture cross-section as a uniformly-pressurized, one-dimensional Griffith crack (Fig. 1a).
2. The crack is ‘closed’ at the advancing fracture edges  $x = \pm\ell(t)$ , i.e. the crack opening is assumed to be zero there. Although seemingly physically sensible, when taken together with the first, negligible-stress-transfer assumption, the ‘closed-edge’ condition can be shown to correspond to the energy release rate into the advancing fracture front, thus rendering the classical PKN - a *zero-toughness* model of an elongated fracture.

Early studies of the classical PKN model (Nordgren, 1972; Kemp, 1990) have been recently revisited and expanded upon by (Kovalyshen and Detournay, 2010; Mishuris et al., 2012; Wrobel and Mishuris, 2015).

While the zero-stress-transfer assumption is approximately valid in the ‘body’ of the elongated fracture, it does break down near the advancing edges  $x = \pm\ell(t)$  where the actual fracture geometry is more adequately approximated by a transition from the plane-strain (‘infinite’-height), fully-elastically-coupled crack geometry at small distances from an edge  $|\ell - x| \ll b$  to the PKN crack geometry away from the edges  $|\ell - x| \gg b$  (Adachi and Peirce, 2008; Dontsov and Peirce, 2016; Peruzzo and Lecampion, 2024). Fortunately, the near-front complications of the full solution are not important on the scale of the entire fracture, as long as the properly reduced front propagation condition(s) for an elongated fracture are imposed. These conditions have been robustly established by Sarvaramini and Garagash (2015), who derived the energy release into the near-front region of an elongated crack and provided the first unambiguous extension of the classic PKN hydraulic fracture model to account for a non-zero fracture toughness. This model is hereafter referred to as the ‘tough PKN’ or ‘tough

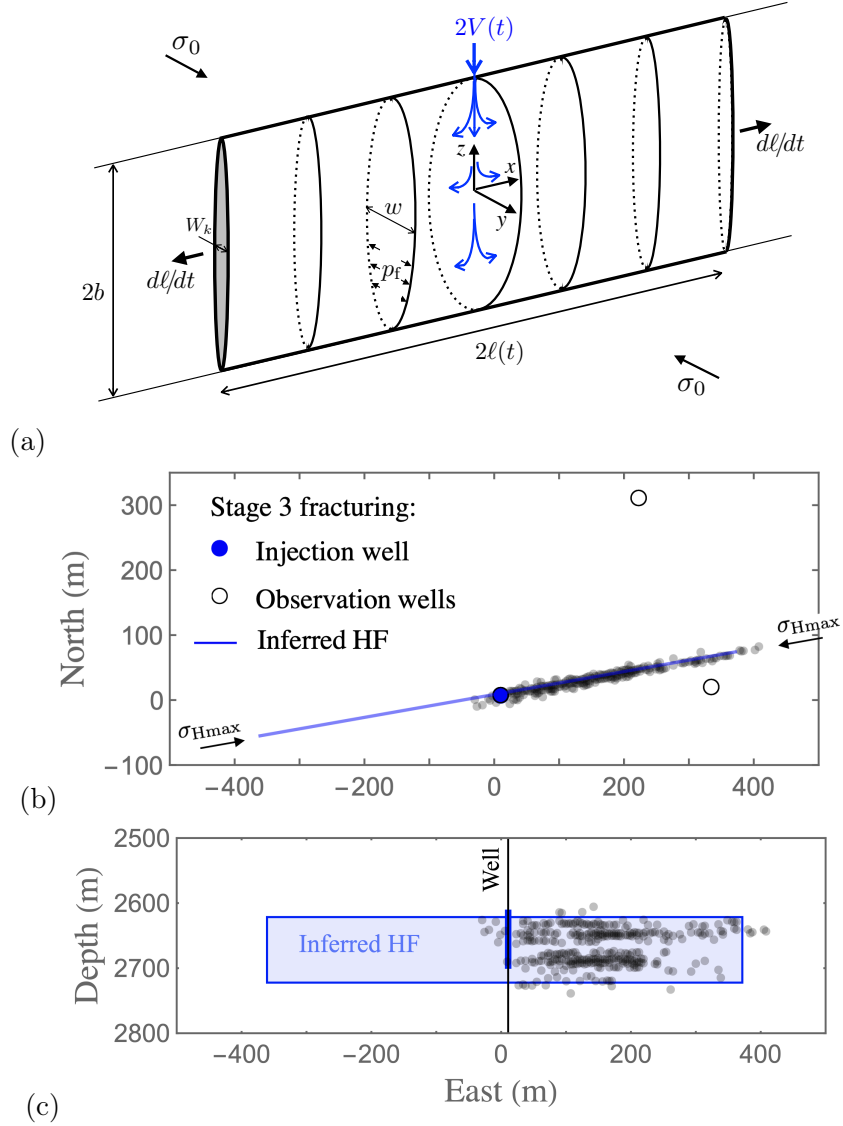


Figure 1: **(a)** Elongated, bi-wing hydraulic fracture of length  $2\ell(t)$  ‘tunneling’ in a layer of height  $2b$ ,  $b \ll \ell$ , driven by fluid injection with cumulative volume  $2V(t)$ . **(b-c)** Relocated micro-seismicity in the top and side (EW) views during Stage 3 hydraulic fracturing injection in vertical well 21-10 in Carthage Cotton Valley Gas Field, Texas (modified after Rutledge et al., 2004; Mayerhofer et al., 2000). Microseismicity is shown by opaque gray dots, such that darker parts of the micro-seismicity ‘cloud’ correspond to higher spatial density of events. Microseismicity, which is induced on natural fractures along the path of the propagating hydraulic fracture, highlights the east wing of an elongated hydraulic fracture with aspect ratio  $b/\ell \approx 1/8$ , (c), aligned in the direction N80E of the maximum regional horizontal stress (Laubach and Monson, 1988), (b). Lack of observed micro-seismicity to the west of the injection well can be due to a distant (eastward) location of the two observation wells in this study, thus, a symmetric bi-wing fracture is assumed here. Rectangle in (c) shows the inferred fracture footprint. Perforated well interval over which the fluid injection took place is shown by a thick blue line in (c).

elongated’ fracture model. In an earlier ad hoc treatment of the toughness problem, Nolte (1991) proposed to ‘fit’ a half-penny-shape crack to the front region of an elongated fracture and to constrain the fluid pressure at the crack tip by requiring the stress intensity factor of the penny-shape crack to match the rock toughness. Rubín and Pollard (1987); Townsend et al. (2017) employed a similar ad hoc approach to model effect of toughness on the lateral propagation of blade-like dikes. Dontsov and Peirce (2016); Peruzzo and Lecampion (2024) validated the ‘tough PKN’ model of Sarvaramini and Garagash (2015) by explicit numerical solutions for the elongated hydraulic fracture propagation with spontaneously evolving front(s). Outside of the realm of fluid-driven fractures, the energy-release-based approach to propagation of elongated cracks have been used to model ‘tunneling’ fractures in layered material composites (Hutchinson and Suo, 1992, and references therein) and large earthquake (shear) ruptures (Weng and Ampuero, 2019).

Chuprakov et al. (2017) has used the tough PKN model of Sarvaramini and Garagash (2015) to investigate numerically the hydraulic fracture propagation after the injection shut-in, when the rock toughness and the fluid leak-off effectively govern the slowing-down fracture propagation towards the ultimate arrest. Dontsov (2022a) have provided a complete analysis of the propagation of a tough elongated hydraulic fracture in the case of a constant rate of fluid injection and accounting for the fluid leak-off, further extending this work to the case of non-Newtonian fracturing fluid in (Dontsov, 2022b). Here, we extend these previous studies to provide a self-consistent analysis of a ‘tough’ elongated fracture driven by arbitrary injection law under assumption of negligible fluid leak-off. We use scaling considerations to identify the non-dimensional parameters governing the propagation regimes and their succession in time, provide a number of analytical solutions in the limiting regimes for arbitrary power-law injection, and posit a simplified, equation-of-motion, approach to solve a general elongated fracture propagation problem.

## 1.2 Rock fracture toughness and scale dependence

It has been long suggested that fracture toughness  $K_{Ic}$  (or corresponding fracture energy  $G_c = K_{Ic}^2/E'$  where  $E'$  is the the plane-strain modulus) scales with fracture size. A number of observations, including that of laboratory fracture (see Liu et al. (2019) for review), field observations of damage zones abating magmatic dikes (Delaney et al., 1986) and reservoir hydraulic fractures (Warpinski et al., 1993), and field inferences based on the scaling of the maximum crack opening with size for veins and dikes (Scholz, 2010; Rivalta et al., 2015, and references therein) and reservoir hydraulic fractures (Shlyapobersky, 1985; Warpinski et al., 1998) can be formally encapsulated in a power law relation

$$K_{Ic} = K_{Ic,0} \left( \frac{b}{b_0} \right)^{\chi/2}, \quad \text{or equivalently} \quad G_c = G_{c,0} \left( \frac{b}{b_0} \right)^{\chi} \quad (1)$$

where  $K_{Ic,0}$  and  $G_{c,0} = K_{Ic,0}^2/E'$  are the reference toughness and fracture energy values at a reference fracture size  $b_0$ , and  $\chi \geq 0$  is the scaling exponent. A particular measure of fracture size  $b$  in (1) is taken as the fracture intermediate dimension for an elongated fracture, i.e. half-height for a laterally-propagating (Fig. 1) or half-breadth for a vertically propagating fracture (e.g. buoyant dikes), respectively. This measure of the fracture size in scaling relation (1) can be generalized to an arbitrary planar fracture geometry, for example, by taking  $b$  as the (local) radius of curvature of the propagating fracture edge.

Experiments constrain toughness of clastic rocks  $K_{Ic,0} \sim 0.5$  to  $1 \text{ MPa m}^{1/2}$  and  $G_{c,0} \sim 10$  to  $30 \text{ Pa m}$  on the laboratory scale  $2b_0 \sim 0.1 \text{ m}$  (Schmidt and Huddle, 1977; Nara et al., 2012; Chandler et al., 2016; Noël et al., 2021, and reference therein). Values of the power-law scaling exponent inferred for geomaterials and wood over a limited range of fracture sizes in a laboratory are  $\chi \approx 0.4$  to  $0.6$  (Morel et al., 2002; Lopez and Schmittbuhl, 1998)), while  $\chi \approx 1$  has been inferred on a much larger scale in the field (e.g., Scholz, 2010). Such parametrized relation (1) is consistent with the *one-to-two order of magnitude increase* in toughness from the lab to the field scale inferred for geo-reservoir hydraulic fracturing (Shlyapobersky, 1985; Warpinski et al., 1998) and magmatic dikes (e.g., Scholz, 2010; Rivalta et al., 2015). It must also be said, however, that the field inferences of the rock fracture toughness may actually lump together the effects of the rock toughness and of the dissipation in the viscous fluid flow in the fracture, thus overestimating the former (e.g., Rivalta et al., 2015; Liu and Lecampion, 2022).

In this study, we develop solutions to a physically-sound model of a ‘tough’ elongated hydraulic fracture that is not limited to a single dissipation mechanism, and thus, when combined with observations, may shed further light on the fracture toughness scaling and its implications to industrial and natural fracturing.

### 1.3 Paper organization

The paper is organized as follows. Section 2 introduces governing equations for a fluid-driven crack tunneling in a layer of fixed height. Section 3 discusses the asymptotics of the solution near the fracture front, emergent limiting fracture propagation regimes, and corresponding regime motivated scaling of the problem. Section 4 presents self-similar solutions for the fracture propagation in the limiting toughness- and viscosity- dominated regimes of propagation for a power-law and exponential fluid injection (including the cases of constant injection volumetric rate, constant injection pressure, and constant injected volume). Section 5 addresses a general transient propagation problem with arbitrary injection schedule by using a simplified equation-of-motion solution method, as well as, a full numerical solution approach. Solution for the shut-in problem is furnished. In Section 6, we discuss the developed solutions to surmise the relative importance of the viscous and toughness related dissipation on the dynamics of an elongated hydraulic fracture during the injection and shut-in stages, respectively, and broach the implications of the toughness scale dependence (1) on the fluid-driven fracture dynamics.

## 2 Governing Equations for Tough Elongated Fluid-Driven Crack

Consider propagation of a hydraulic fracture driven by the injection of fluid volume  $2V(t)$  and constrained in height to a layer of thickness  $2b$  (Fig. 1a). The crack is internally loaded by distributed fluid pressure  $p_f(x)$  and remotely confined by minimum in-situ compressive stress  $\sigma_o$ . The fracture geometry is therefore set by the expanding crack length  $2\ell(t)$  and constant height  $2b$ . For an elongated crack,  $b \ll \ell$ , crack opening in a given  $x$  cross-section is approximated by the Griffith’s solution for a plane-strain, uniformly-pressurized crack,  $w(x, z) = (4p(x)/E')\sqrt{b^2 - z^2}$ , where  $E' = E/(1 - \nu^2)$  is the plane-strain elastic modulus. Unidirectional flow inside the crack of an incompressible fluid with viscosity  $\mu$  is governed by

Poiseuille's law,  $v(x, z) = -(w^2(x, z)/12\mu)(\partial p/\partial x)$ , and continuity,

$$\frac{\partial w}{\partial t} + \frac{\partial wv}{\partial x} = 0. \quad (2)$$

We define height-averages  $w(x)$  and  $v(x)$  of the local crack opening  $w(x, z)$  and fluid velocity  $v(x, z)$

$$w(x) = \frac{1}{2b} \int w(x, z) dz = \frac{bp(x)}{\bar{E}}, \quad v(x) = \frac{1}{2bw(x)} \int w(x, z)v(x, z) dz = -\frac{w^2(x)}{\bar{\mu}} \frac{\partial p}{\partial x} \quad (3)$$

in terms effective modulus  $\bar{E} = E'/\pi$  and viscosity  $\bar{\mu} = \pi^2\mu$ . Substituting expression for  $p$  from the first into the second equation in the above, we get a convenient form of the lubrication equation for the tunneling crack

$$v(x) = -\frac{\bar{E}}{3\bar{\mu}b} \frac{\partial w^3(x)}{\partial x} \quad (4)$$

Boundary conditions at the fracture tip  $x = \ell(t)$  and inlet  $x = 0$  for the above set of field equations are formulated in the following, while making use of the problem symmetry about the inlet.

- Fluid continuity at the tip,

$$x = \ell : \quad v = \dot{\ell} \quad (5)$$

Here  $\dot{\ell} = d\ell/dt$  is the propagation velocity.

- Fluid continuity at the inlet,

$$x = 0 : \quad 2b w v = \dot{V} \quad (6)$$

Here  $V$  and  $\dot{V} = dV/dt$  are the (half) injection volume and its rate, respectively. Inlet condition (6) can be replaced by the global continuity statement

$$\int_0^\ell 2b w dx = V \quad (7)$$

- Sarvaramini and Garagash (2015) established that elastic energy release  $dU$  to advance the tunneling fracture front by  $d\ell > 0$  is approximately  $dU \approx U_{2D}(\ell)d\ell$ , where  $U_{2D}(\ell) = b^2 p^2(\ell)/\bar{E}$  is the internal energy of a two-dimensional (plain-strain, Griffith) crack of extent  $b$  uniformly pressurized by net-pressure value  $p(\ell)$  at the front of the tunneling crack. The front-average elastic energy release rate is then  $G = dU/(2bd\ell) = bp^2(\ell)/(2\bar{E})$ . Quasi-static fracture propagation requires that the energy release rate  $G$  is equal to the fracture energy  $G_c$ , which can be related to the more-commonly used solid toughness  $K_{Ic}$  by  $G_c = K_{Ic}^2/E'$ . In view of the above expression for  $G$ , the propagation condition  $G = G_c$  constrains the value of the net-pressure at the fracture front to the critical value  $P_k$ ,

$$x = \ell : \quad p = P_k \equiv \frac{\bar{K}}{\sqrt{b}}, \quad (8)$$

where  $\bar{K} = \sqrt{2/\pi}K_{Ic}$  is an effective toughness parameter. Alternatively, the above propagation condition can be expressed in terms of the opening, see the first in (3), attaining a critical value  $W_k$  at the fracture front:

$$x = \ell : \quad w = W_k \equiv \frac{\bar{K}\sqrt{b}}{\bar{E}}. \quad (9)$$

The opening at the front of an elongated fracture is therefore finite as long as the material toughness is. This apparently non-physical condition is reconciled by considering that the presented model is an adequate approximation for an elongated fracture starting only from some distance away from the propagating edge, more specifically at distances greater than the crack height  $2b$ . In other words, the model provides an ‘outer’ solution to the elongated crack problem, i.e. the solution outside of the immediate vicinity of the propagating tips, which does not have to satisfy the physical constraints at the actual fracture tip, e.g. that of zero opening there. Full numerical solutions of hydraulic fracture propagation with constrained height (Dontsov and Peirce, 2016; Peruzzo and Lecampion, 2024)<sup>1</sup> validate the applicability of the simplified elongated crack model with propagation condition (8). We also observe that the PKN model (which is equivalent to equations (4-7) with the additional condition of zero crack opening at the propagating edges), is recovered from the current model in the limit of zero toughness.

In summary, propagation of an elongated hydraulic fracture is governed by continuity (2) and lubrication (4) phrased in terms of height-averaged  $w$  and  $v$ , (3), and the boundary conditions at the fracture tip, (5) and (9), and the inlet, (6) or (7). Solution of the model is parametrized by fracture height  $2b$ , injected fluid volume history  $2V(t)$  and the three effective material parameters (elastic modulus, fluid viscosity, and toughness),

$$\bar{E} = \frac{1}{\pi} \frac{E}{1 - \nu^2}, \quad \bar{\mu} = \pi^2 \mu, \quad \bar{K} = \sqrt{\frac{2}{\pi}} K_{Ic}. \quad (10)$$

### 3 Tip Asymptotics and Scaling

Integrating lubrication (4) near the fracture tip, where  $v \approx \dot{\ell}$ , (5), and further applying propagation condition, (9), allows to express the crack opening asymptote there as,

$$x \rightarrow \ell : \quad w = \left( W_k^3 + W_m^3 \frac{\ell - x}{\ell} \right)^{1/3}, \quad (11)$$

where  $W_k$ , given in (9), and

$$W_m = \left( \frac{3\bar{\mu}b}{\bar{E}} \ell \dot{\ell} \right)^{1/3} \quad (12)$$

can be identified as characteristic values of the crack opening under the toughness and viscosity dominated conditions, respectively. Indeed, setting  $\bar{\mu} = 0$  in the *toughness-dominated regime*, we have  $w(x, t) = W_k$  near the tip (and, as shown further, everywhere along the crack), while setting  $K_{Ic} = 0$  in the *viscosity-dominated regime*, we recover  $w(x, t) = W_m(t) (1 - x/\ell(t))^{1/3}$

---

<sup>1</sup>where fracture height growth is not precluded, but limited by the presence of the stress barriers, such that the blade-like geometry  $b(x, t) \ll \ell(t)$  is maintained.

near the tip (Kemp, 1990; Kovalyshen and Detournay, 2010). Therefore, in general, these two limiting regimes can be identified by comparing magnitudes of  $W_k$  and  $W_m$ . It follows from definitions (9) and (12), that, when neither fluid viscosity nor the solid fracture toughness are exactly zero and since  $W_k$  is independent of time, fracture evolves towards the viscosity (toughness) dominated regime if the crack grows faster (slower) than  $\ell \sim \sqrt{t}$ , i.e.,  $W_m$  is increasing (decreasing) function of time. General problem of the crack evolution can be therefore cast in terms of the transition between these two limiting regimes.

It is useful for further solution development to introduce two scaling schemes for the general solution, as suggested by the toughness- and viscosity- dominated end-member cases introduced in the above. Let us define normalized opening/net-pressure  $\Omega$ , fluid velocity  $\vartheta$ , and crack length  $\gamma$  as functions of normalized coordinate  $\xi = x/\ell(t)$  and time:

$$w(x, t) = (b/\bar{E})p(x, t) = W(t)\Omega(\xi, t), \quad v(x, t) = \dot{\ell}(t)\vartheta(\xi, t), \quad \ell(t) = L(t)\gamma(t) \quad (13)$$

with the characteristic opening  $W$  and length  $L$  scales given by

$$W(t) = \begin{cases} W_k = \bar{K}\sqrt{b/\bar{E}} & \text{(toughness scaling)} \\ W_m(t) = (3\bar{\mu}b\ell\dot{\ell}/\bar{E})^{1/3} & \text{(viscosity scaling)} \end{cases}, \quad L(t) = \frac{V(t)}{2bW(t)}, \quad (14)$$

We note that since  $W_m$  is defined in terms of the unknown crack length  $\ell$ , the corresponding expression (14) for the characteristic length  $L_m$  in the viscosity scaling is implicit, and furthermore is dependent upon the complete solution.

Substituting (13)-(14) into the local continuity (2) yields the normalized equation

$$t\dot{\Omega} + \frac{t\dot{W}}{W}\Omega - \frac{t\dot{\ell}}{\ell} \left( \xi \frac{\partial \Omega}{\partial \xi} - \frac{\partial \Omega \vartheta}{\partial \xi} \right) = 0 \quad (15)$$

or, in alternative form, obtained by integrating in space, using crack tip continuity,  $\vartheta|_{\xi \rightarrow 1} = 1$ , and resolving for the fluid velocity,

$$\vartheta = \xi - \frac{1}{\Omega} \int_1^\xi \left( \Omega + \frac{t\dot{\Omega} + \frac{t\dot{W}}{W}\Omega}{t\dot{\ell}/\ell} \right) d\xi \quad (16)$$

where

$$\frac{t\dot{\ell}}{\ell} = \frac{t\dot{L}}{L} + \frac{t\dot{\gamma}}{\gamma} = \frac{t\dot{V}}{V} - \frac{t\dot{W}}{W} + \frac{t\dot{\gamma}}{\gamma} \quad (17)$$

and the time derivatives in the normalized equations are carried out at a fixed  $\xi$ .

Normalized form of the fluid continuity at the inlet (6) is

$$(\Omega\vartheta)|_{\xi=0} = \frac{t\dot{V}/V}{t\dot{\ell}/\ell} \frac{1}{\gamma} \quad (18)$$

while, equivalently, the normalized form of global continuity (2) is

$$\int_0^1 \Omega d\xi = \frac{1}{\gamma} \quad (19)$$

Normalized lubrication equation (4) and the tip asymptote (11), which embodies both the tip fluid continuity (5) and the tip propagation (9) conditions, in the two scalings read:

$$\text{toughness scaling: } \vartheta = -\frac{1}{\mathbb{M}} \frac{\partial \Omega^3}{\partial \xi}, \quad \Omega_{|\xi \rightarrow 1} = (1 + \mathbb{M}(1 - \xi))^{1/3}, \quad (20)$$

$$\text{viscosity scaling: } \vartheta = -\frac{\partial \Omega^3}{\partial \xi}, \quad \Omega_{|\xi \rightarrow 1} = (\mathbb{K}^3 + 1 - \xi)^{1/3}. \quad (21)$$

where normalized crack front parameters  $\mathbb{K}$  and  $\mathbb{M}$  are defined in terms of the ratio of the two characteristic opening scales (14),

$$\mathbb{K} = \frac{W_k}{W_m} = \frac{\bar{K} b^{1/6}}{(3\bar{\mu}\bar{E}^2 \ell \dot{\ell})^{1/3}}, \quad \mathbb{M} = \frac{W_m^3}{W_k^3} = \frac{3\bar{\mu}\bar{E}^2 \ell \dot{\ell}}{\bar{K}^3 b^{1/2}}. \quad (22)$$

Non-dimensional crack opening, half-length, and fluid velocity in the two scalings are simply inter-related,

$$\frac{\Omega_m}{\Omega_k} = \frac{\gamma_k}{\gamma_m} = \frac{W_k}{W_m} = \frac{L_m}{L_k} = \mathbb{K} = \mathbb{M}^{-1/3}, \quad \frac{\vartheta_m}{\vartheta_k} = 1 \quad (23)$$

where indices refer to a particular scaling used.

Nondimensional parameters (22) characterize the relative importance of the corresponding energy dissipation mechanisms in hydraulic fracturing with constrained height, such that one can formally define the viscosity-dominated ( $\mathbb{K} \ll 1$ ) and the toughness-dominated ( $\mathbb{M} \ll 1$ ) propagation regimes.

### 3.1 Alternate, Explicit Viscosity Scaling

Viscosity scaling introduced in the above is implicit, since the scales for the opening,  $W_m$ , and length,  $L_m$ , depend on the unknown crack half-length and its time derivative (propagation speed). It will therefore be useful to introduce an alternative, explicit set of scales,  $\bar{W}_m$  and  $\bar{L}_m$ , which are independent of the sought solution, by writing

$$W_m = (t\dot{\ell}/\ell)^{1/5} \gamma_m^{2/5} \bar{W}_m, \quad L_m = (t\dot{\ell}/\ell)^{-1/5} \gamma_m^{-2/5} \bar{L}_m \quad (24)$$

where

$$\bar{W}_m = \left( \frac{3\bar{\mu}V^2(t)}{4\bar{E}bt} \right)^{1/5}, \quad \bar{L}_m = \frac{V(t)}{2b\bar{W}_m} = \left( \frac{\bar{E}V^3(t)t}{24\bar{\mu}b^4} \right)^{1/5}, \quad (25)$$

Using (24) in (22), we can write for the implicit normalized toughness  $\mathbb{K}$  and viscosity  $\mathbb{M}$  parameters

$$\mathbb{K} = (t\dot{\ell}/\ell)^{-1/5} \gamma_m^{-2/5} \mathcal{K}, \quad \mathbb{M} = (t\dot{\ell}/\ell) \gamma_k^2 \mathcal{M}, \quad (26)$$

in terms of alternative explicit normalized toughness  $\mathcal{K}$  and viscosity  $\mathcal{M} = \mathcal{K}^{-5}$  parameters defined as

$$\mathcal{K} = \frac{W_k}{\bar{W}_m} = \left( \frac{4\bar{K}^5 b^{7/2} t}{3\bar{\mu}\bar{E}^4 V^2(t)} \right)^{1/5}, \quad \mathcal{M} = \left( \frac{\bar{W}_m}{W_k} \right)^5 = \frac{3\bar{\mu}\bar{E}^4 V^2(t)}{4\bar{K}^5 b^{7/2} t}. \quad (27)$$

In (24) and (24),  $\gamma_{m,k} = \ell/L_{m,k}$  is the previously-defined, normalized half-length in either the implicit-viscosity ( $m$ ) or toughness ( $k$ ) scaling.

Using explicit viscosity scales to define the corresponding normalized opening/net pressure and crack half-length similar to (13),

$$w(x, t) = (b/\bar{E})p(x, t) = \bar{W}_m(t)\bar{\Omega}_m(\xi, t), \quad \ell(t) = \bar{L}_m(t)\bar{\gamma}_m(t), \quad (28)$$

the normalized solutions in the implicit and explicit viscosity scalings can then be related as

$$\frac{\gamma_m}{\bar{\gamma}_m} = \frac{\bar{\Omega}_m}{\Omega_m} = \frac{\mathcal{K}}{\mathbb{K}} = (t\dot{\ell}/\ell)^{1/3} \bar{\gamma}_m^{2/3} \quad (29)$$

## 4 Limiting Self-Similar Solutions

### 4.1 Zero-Viscosity Solution

In the toughness-dominated regime, the solution is given by the *zero-viscosity solution* of the set of equations (2-9) or, in the normalized form, (15)-(20). The solution is particularly simple,- it is given in the *toughness scaling* by

$$\mathbb{M} = 0 : \quad \Omega_k(\xi) = \gamma_k = 1.$$

where subscript  $k$  points to the scaling used. In the dimensional form,

$$\mu = 0 : \quad w(x, t) = (b/\bar{E})p(x, t) = W_k, \quad \ell(t) = L_k(t) = \frac{V(t)}{2bW_k}, \quad (30)$$

it corresponds to uniformly pressurized and open crack, which extent is proportional to the injected fluid volume.

It also proves convenient to formulate the *small viscosity correction* to the above zero-viscosity solution by considering the first term in the solution expansion in  $\mathbb{M} \ll 1$ . Using standard asymptotic methods (see, e.g., a similar treatment of the plane-strain hydraulic fracture (Garagash, 2006)), we can find for power-law fluid injection,  $V \propto t^\alpha$ ,

$$\text{injection, } \alpha > 0 : \quad \Omega_k \approx (1 + \mathbb{M}(1 - \xi))^{1/3}, \quad \gamma_k \approx 1 - \frac{1}{6}\mathbb{M}, \quad \mathbb{M} \approx \alpha\mathcal{M} \quad (31)$$

$$\text{fixed-volume, } \alpha = 0 : \quad \Omega_k \approx \left(1 + \mathbb{M}\frac{2}{\pi} \cos \frac{\pi\xi}{2}\right)^{1/3}, \quad \gamma_k \approx 1 - \frac{4}{3\pi^2}\mathbb{M}, \quad \mathbb{M} \sim \exp\left(-\frac{3\pi^2}{4\mathcal{M}}\right) \quad (32)$$

### 4.2 Zero-Toughness Solution

#### Similarity Considerations in Viscosity Scaling

Normalized equations in *viscosity scaling*, (15)-(19) and (21), admit self-similar solutions, i.e.  $\Omega_m = \Omega_m(\xi)$  and  $\gamma_m = \text{const}$ , when (*i*) dimensionless toughness parameter  $\mathbb{K}$  is time-independent; and (*ii*) fluid injection is either a power-law or an exponential of time.

Focusing on a *power-law injection* first, the explicit scales (25) and toughness parameter (27) are also power-laws,

$$V \propto t^\alpha : \quad \bar{L}_m \propto t^{(3\alpha+1)/5}, \quad \bar{W}_m \propto t^{(2\alpha-1)/5}, \quad \mathcal{K} \propto t^{-(2\alpha-1)/5}, \quad (33)$$

and, in view of self-similarity ( $\gamma_m = \text{const}$ ), so are the corresponding implicit scales (24) and toughness parameter (26)

$$V \propto t^\alpha : \quad \frac{L_m}{\bar{L}_m} = \frac{\bar{W}_m}{W_m} = \frac{\mathbb{K}}{\mathcal{K}} = \left( \frac{3\alpha + 1}{5} \right)^{-1/5} \gamma_m^{-2/5} = \text{const}. \quad (34)$$

(Here we have used the similarity notion  $\dot{\gamma}_m = 0$  to reduce (17) to  $t\dot{\ell}/\ell = t\dot{L}_m/L_m = t\dot{\bar{L}}_m/\bar{L}_m = (3\alpha + 1)/5$ ). These allow to reduce the continuity, (15), and lubrication, the first in (21), equations to an ordinary differential equation (ODE) in  $\xi$ ,

$$\frac{2\alpha - 1}{3\alpha + 1} \Omega_m - \left( \xi \frac{d\Omega_m}{d\xi} - \frac{d\Omega_m \vartheta_m}{d\xi} \right) = 0 \quad \text{with} \quad \vartheta_m = -\frac{d\Omega_m^3}{d\xi}, \quad (35)$$

This equation can be solved together with boundary conditions,  $\Omega_m(1) = \mathbb{K}$  and  $\vartheta_m(1) = 1$ , for the normalized opening distribution  $\Omega_m(\xi)$ . The normalized half-length can then be obtained by integrating (19),  $\gamma_m = 1/\int_0^1 \Omega_m(\xi) d\xi$ .

Requirement of time-invariance of the dimensionless toughness  $\mathbb{K}$ , i.e. self-similarity condition (i) in the above, is satisfied when either

- $\mathbb{K} = 0$ , i.e. when material toughness is zero  $K_{Ic} = 0$  and injection law is arbitrary, or
- $\mathbb{K} = \text{const}$ , when material toughness  $K_{Ic}$  is arbitrary and injection law is particular,  $V(t) \propto t^\alpha$  with  $\alpha = 1/2$ . This case corresponds to *injection at constant inlet fluid pressure*,  $p(0) = \text{const}$ , constant inlet opening,  $w(0) = \text{const}$ , and square-root-time expansion of the crack front  $\ell \propto t^{1/2}$  - see (33) for the time-dependence of the corresponding scales.

For an *exponential injection*, we can establish for the implicit scales  $L_m$  and  $W_m$ , and the toughness parameter  $\mathbb{K}$  relationships similar to those for the power-law case in the above,

$$V \propto e^{t/t_*} : \quad \frac{L_m}{\bar{L}_m^*} = \frac{\bar{W}_m^*}{W_m} = \frac{\mathbb{K}}{\mathcal{K}^*} = \left( \frac{3}{5} \right)^{-1/5} \gamma_m^{-2/5} = \text{const}. \quad (36)$$

where the newly defined explicit time-dependent scales  $\bar{L}_m^*$  and  $\bar{W}_m^*$  and toughness  $\mathcal{K}^*$  for the exponential injection case are

$$\bar{L}_m^*(t) = \bar{L}_m(t_*) e^{3(t/t_* - 1)/5}, \quad \bar{W}_m^*(t) = \bar{W}_m(t_*) e^{2(t/t_* - 1)/5}, \quad \mathcal{K}^*(t) = \mathcal{K}(t_*) e^{-2(t/t_* - 1)/5} \quad (37)$$

Here  $t_* > 0$  is injection timescale and the self-similarity is assumed, i.e.  $\gamma_m$  is a time-independent constant. Above scaling relations show that length and opening evolve with time as  $\sim e^{3t/5t_*}$  and  $\sim e^{2t/5t_*}$ , respectively, while dependence on time of the dimensionless toughness is reversed  $\sim e^{-2t/5t_*}$ . Self-similarity, which requires  $\mathbb{K}$  to be a time-invariant constant, can therefore only be achieved when that constant is zero,  $\mathbb{K} = 0$ . This is realized for all times when material toughness is zero  $K' = 0$  or asymptotically at times  $t \gtrsim t_*$  when

$K_{Ic} > 0$ . In view of (36), local continuity and lubrication can be shown to be formally equivalent to the power-law ones (35) with  $\alpha \rightarrow \infty$ , i.e. with  $(2\alpha - 1)/(3\alpha + 1) \rightarrow 2/3$  in the first term in (35). In other words, the dimensionless zero-toughness solution,  $\Omega_m(\xi)$  and  $\gamma_m$ , for exponential injection is given by that for the power-law case in the  $\alpha \rightarrow \infty$  limit<sup>2</sup>.

### Particular Zero-Toughness Solutions for $\alpha = 0$ and $\alpha = 4/3$

Differential equation (35) has an analytical zero-toughness solution for specific values of  $\alpha$ , that is when  $\alpha = 0$  in the fixed-volume-case, and when  $\alpha = 4/3$ , which is a particular injection scenario corresponding to a constant rate of crack growth ( $\bar{L}_m \propto t$ ), respectively. These two solutions are:

$$\text{fixed-volume, } \alpha = 0 : \quad \Omega_m = \left( \frac{1 - \xi^2}{2} \right)^{1/3}, \quad \vartheta_m = \xi, \quad \gamma_m = 1.49757, \quad (38)$$

$$\text{fixed-propagation-rate, } \alpha = 4/3 : \quad \Omega_m = (1 - \xi)^{1/3}, \quad \vartheta_m = 1, \quad \gamma_m = 4/3, \quad (39)$$

where  $\vartheta(\xi)$  and  $\gamma$  were evaluated from (21) and (19), respectively.

### General Zero-Toughness Solution

General zero-toughness solutions for arbitrary injection power-law can be obtained by series expansion. As already pointed out, the original PKN formulation corresponds to the zero-toughness limit of the model suggested here. The first treatment of this case is due to Nordgren (1972), and its complete solution for a constant fluid injection rate ( $\alpha = 1$ ) was first formulated by Kemp (1990).

Kemp's solution can be generalized to arbitrary injection power law  $V \propto t^\alpha$  with  $\alpha > 0$  as

$$\Omega_m = (1 - \xi)^{1/3} \sum_{j=0}^{\infty} A_j(\alpha)(1 - \xi)^j, \quad \gamma_m^{-1} = \int_0^1 \Omega_m d\xi = \frac{3}{4} \sum_{j=0}^{\infty} \frac{A_j(\alpha)}{1 + 3j/4} \quad (40)$$

Coefficients  $A_j(\alpha)$  are obtained by substituting the opening series into lubrication equation (35) and expanding the result near the tip,  $\xi = 1$ ,

$$A_0 = 1, \quad A_1 = \frac{3\alpha/4 - 1}{6(3\alpha + 1)}, \quad A_2 = \frac{(3\alpha/4 - 1)(1 - 51\alpha/28)}{6^2(3\alpha + 1)^2}, \dots$$

where  $j = 0$  term provides the tip asymptote (20). It is evident that  $A_{j \geq 1} \propto 3\alpha/4 - 1$ , thus, validating that  $j = 0$  term corresponds to the exact solution in the particular case of  $\alpha = 4/3$ , see (39).

Examination of the series convergence (Fig. 2) shows that the single-term-solution, i.e.  $\Omega_m \approx (1 - \xi)^{1/3}$  and  $\gamma_m^{-1} \approx 3/4$ , provides a very good approximation for the half-length and opening (within 1%) for injections at a non-decreasing rate in time,  $\alpha \geq 1$ , while approximation becomes progressively less adequate for decreasing value of  $\alpha < 1$ . Furthermore, Fig. 2 shows

<sup>2</sup>This equivalence is for the non-dimensional solutions only. Corresponding dimensional solutions are distinct, as they are recovered from the non-dimensional ones by applying the distinct sets of time-dependent scales  $W_m$  and  $L_m$ , given by (36) and (34) for exponential and power-law injections, respectively.

that the two-term-solution,  $\Omega_m \approx (1 - \xi)^{1/3} + A_1(\alpha)(1 - \xi)^{4/3}$  and  $\gamma_m^{-1} \approx 3/4 + 3A_1(\alpha)/7$ , gives the half-length within 1% for the entire range of injection exponent  $\alpha \geq 0$ .

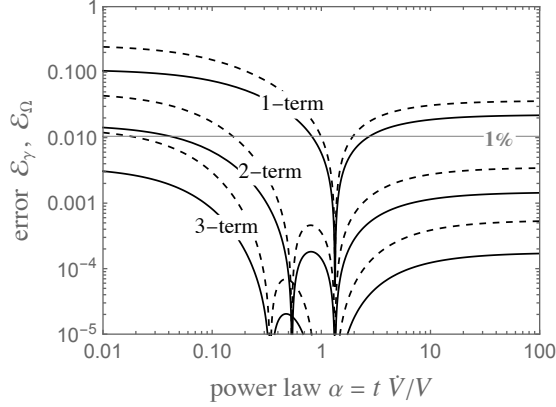


Figure 2: Power-law injection, zero-toughness. Relative error for the fracture half-length (solid) and opening at the inlet (dashed) of the series solution (40) when truncated to one, two, and three terms, respectively, as a function of injection power-law  $\alpha$ .

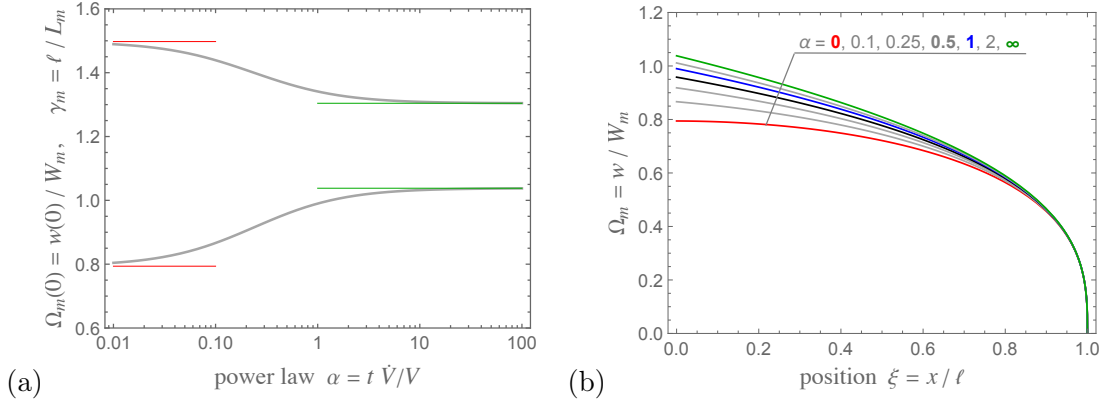


Figure 3: Power-law injection, zero-toughness solution in the *implicit viscosity scaling*, (40). (a) Normalized opening/net-pressure at the inlet  $\Omega_m(0) = w(0)/W_m = p(0)/(\bar{E}W_m/b)$  and crack half-length  $\gamma_m = \ell/L_m$  as a function of injection power-law  $\alpha$ ,  $V(t) \propto t^\alpha$ . The fixed-volume  $\alpha = 0$  and equivalent exponential  $\alpha = \infty$  limits are indicated by thin lines. (b) Distribution of the normalized opening/net-pressure  $\Omega_m = w/W_m$  along the crack as a function of normalized position  $\xi = x/\ell$ , from the inlet  $\xi = 0$  to the tip  $\xi = 1$ , for various values of  $\alpha$ .

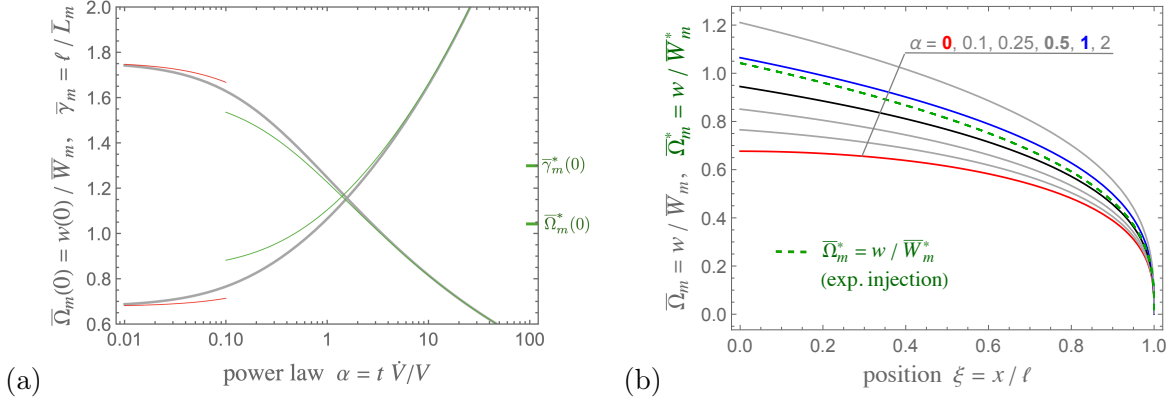


Figure 4: Power-law injection, zero-toughness solution (Fig. 3) rescaled to the *explicit viscosity scaling*. (a) Normalized opening/net-pressure at the inlet  $\bar{\Omega}_m(0) = w(0)/\bar{W}_m = p(0)/(\bar{E}\bar{W}_m/h)$  and crack half-length  $\bar{\gamma}_m = \ell/\bar{L}_m$  as a function of injection power-law  $\alpha$ ,  $V(t) \propto t^\alpha$ . Small and large  $\alpha$  asymptotes are shown by thin lines. (b) Distribution of the normalized opening/net-pressure along the crack,  $\bar{\Omega}_m = w/\bar{W}_m$  for a power-law  $0 \leq \alpha < \infty$  and  $\bar{\Omega}_m^* = w/\bar{W}_m^*$  for an exponential injection, as a function of normalized position  $\xi = x/\ell$ . Dependence of the solution on time follows from that of the scales:  $\bar{W}_m(t) = (3\bar{\mu}V^2(t)/4\bar{E}bt)^{1/5} \propto t^{(2\alpha-1)/5}$  and  $\bar{L}_m(t) = V(t)/(2b\bar{W}_m(t)) \propto t^{(3\alpha+1)/5}$  for a power-law, and  $\bar{W}_m^*(t) = \bar{W}_m(t_*)e^{2(t/t_*-1)/5}$  and  $\bar{L}_m^*(t) = \bar{L}_m(t_*)e^{3(t/t_*-1)/5}$  for an exponential-law injection.

Zero-toughness solution in the entire range of power-law exponent  $\alpha$ ,  $0 \leq \alpha \leq \infty$ , is shown in Fig. 3. Fig. 3a shows the normalized crack length  $\gamma_m$  and opening at the inlet  $\Omega_m(0)$  as a function of the power-law  $\alpha$ . Spatial distribution of the normalized fracture opening is shown on Fig. 3b for various values of  $\alpha$ .

Normalized zero-toughness solution, (40) and Fig. 3, is expressed in terms of implicit scales  $L_m$  and  $W_m$ , (24). Corresponding normalized solution using explicit scales  $\bar{L}_m$  and  $\bar{W}_m$ , (28), and, therefore, subsequently corresponding *dimensional solution* can be readily obtained from relation (34) for power-law injection ( $0 \leq \alpha < \infty$ ), and from similar relation (36-37) for exponential injection ( $\alpha = \infty$ ). For example, for the explicit dimensionless half-length  $\bar{\gamma}_m = \ell/\bar{L}_m = (5/(3\alpha+1))^{1/5}\gamma_m^{3/5}$  for power-law and  $\bar{\gamma}_m = \ell/\bar{L}_m^* = (5/3)^{1/5}\gamma_m^{3/5}$  for exponential injection. Resulting explicit dimensionless zero-toughness solution is plotted on Fig. 4.

Table 1 lists numerical values accurate to at least six significant digits of the normalized solution for the fracture half-length and opening at the inlet, in both the implicit and explicit scales, for various values of injection power-law exponent. We particularly highlight solutions for practically-relevant injection scenarios corresponding to injections with fixed volume ( $\alpha = 0$ ), constant injection pressure ( $\alpha = 1/2$ ), constant volume-rate ( $\alpha = 1$ ), and exponentially increasing volume, rate thereof, and injection pressure ( $\alpha = \infty$ ).

Table 1: Zero-toughness solution for the dimensionless fracture half-length and opening/net-pressure at the inlet using implicit,  $\gamma_m = \ell/L_m$  and  $\Omega_m(0) = w(0)/W_m = p(0)/(\bar{E}W_m/b)$ , and explicit,  $\bar{\gamma}_m = \ell/\bar{L}_m$  and  $\bar{\Omega}_m(0) = w(0)/\bar{W}_m = p(0)/(\bar{E}\bar{W}_m/b)$ , scales for various values of injection power-law  $\alpha$  ( $V \propto t^\alpha$ ). For exponential injection ( $V \propto e^{t/t^*}$ ), the implicit dimensionless solution is given by that for the power-law one with  $\alpha \rightarrow \infty$ , while the explicit dimensionless solution is using amended explicit length and opening scales,  $\bar{\gamma}_m = \ell/\bar{L}_m^*$  and  $\bar{\Omega}_m(0) = w(0)/\bar{W}_m^* = p(0)/(\bar{E}\bar{W}_m^*/b)$ . The two sets of length and opening scales are related via (34) for power-law injection, and by (36-37) for exponential injection.

Power-law $\alpha$	Description	Implicit		Explicit	
		$\gamma_m$	$\Omega_m(0)$	$\bar{\gamma}_m$	$\bar{\Omega}_m(0)$
<b>0</b>	fixed injection volume	1.49757	0.79370	1.75815	0.67607
0.1		1.43910	0.86642	1.62877	0.76553
0.25		1.39748	0.91836	1.50797	0.85107
<b>1/2</b>	fixed injection pressure	1.36597	0.95815	1.38506	0.94494
<b>1</b>	fixed injection volume rate	1.34113	0.98993	1.24699	1.06466
4/3	fixed crack propagation rate	1.33333	1.00000	1.18840	1.12196
2		1.32469	1.01121	1.10674	1.21036
<b><math>\infty</math></b>	exponential injection	1.30424	1.03802	1.29893	1.04227

## 5 Transient Solutions

When considering a fracture propagating in the rock with finite toughness, the solution is bound to evolve in time between the two limiting propagation regimes discussed in Section 4. More specifically, given the dependence of the normalized viscosity on time,  $\mathcal{M} \propto V^2(t)/t$ , this evolution will take place from the initially toughness-dominated to the eventually viscosity-dominated regime when injection is fast enough (injected volume  $V(t)$  increases faster than  $\sqrt{t}$ ), and the reversed evolution, from the viscosity- towards the toughness- domination with time, will take place when the injection is slow enough ( $V(t)$  increases slower than  $\sqrt{t}$ ). The former is true, for example, for injection with fixed rate,  $\mathcal{M} \propto t$ , while the latter, e.g., for injection with fixed volume,  $\mathcal{M} \propto 1/t$ . The threshold injection law,  $V \propto \sqrt{t}$  and  $\mathcal{M} = \text{const}$ , which separates the two types of evolutionary behavior, corresponds to injection with fixed source pressure.

A numerical solution of the fracture evolution in space-time to any desired degree of accuracy can be obtained by means of the method-of-lines, which relies on a discretization of the governing equations in space and then solving resulting system of ODEs at the spatial nodes continuously in time (see Appendix A for details). As an alternative to this fully-numerical solution, we also propose an approximate *Equation-of-Motion* (EofM) for the elongated hydraulic fracture - a single ODE in time which allows for a simplified, accurate and very expedient approximate solution.

In this Section, we formulate the EofM approach first and then provide both the fully-numerical and the EofM transient solutions for (i) power-law-injection, and (ii) injection at a constant rate followed by the shut-in.

## 5.1 Approximate Equation-of-Motion

To facilitate a simplified solution approach, we choose to approximate the crack opening spatiotemporal evolution by the form suggested by the small-viscosity solution, given in the *toughness scaling* by the firsts in (31) and (32), respectively, and repeated below together with the resulting approximation for the normalized fluid velocity  $\vartheta_k = -\partial\Omega_k^3/\partial\xi$ ,

$$\text{injection, } \dot{V} > 0: \quad \Omega_k(\mathbb{M}, \xi) \approx (1 + \mathbb{M}(1 - \xi))^{1/3}, \quad \vartheta_k(\xi) \approx 1 \quad (41)$$

$$\text{fixed-volume, } \dot{V} = 0: \quad \Omega_k(\mathbb{M}, \xi) \approx \left(1 + \mathbb{M} \frac{2}{\pi} \cos \frac{\pi\xi}{2}\right)^{1/3}, \quad \vartheta_k(\xi) \approx \sin \frac{\pi\xi}{2} \quad (42)$$

Time-dependence of the approximate solution follows solely from that of the normalized, implicit viscosity parameter  $\mathbb{M}(t)$ . Contrary to the small-viscosity asymptote, here  $\mathbb{M}(t)$  is not necessarily small and is an unknown (part of the solution). We note in passing, that the chosen opening approximation can also be framed as an approximate continuation of the tip asymptote, the second in (20), to the remainder of the crack, that is respecting the inlet (flow/no-flow) boundary condition. Latter approach was originally used in (Garagash, 2019; Dontsov, 2016, 2017; Garagash, 2022) to formulate EofM for plane-strain and radial hydraulic fractures.

Corresponding approximation for the normalized crack length,  $\gamma_k = \ell/L_k$ , follows by evaluating the global fluid continuity (19) for the assumed form for the opening, (41)-(42),

$$\gamma_k \approx \mathcal{Y}(\mathbb{M}) = \left(\int_0^1 \Omega_k(\mathbb{M}, \xi) d\xi\right)^{-1} \quad (43)$$

where

$$\begin{aligned} \text{injection, } \dot{V} > 0: \quad \mathcal{Y}(\mathbb{M}) &= \frac{4}{3} \frac{\mathbb{M}}{(1 + \mathbb{M})^{4/3} - 1} \\ \text{fixed-volume, } \dot{V} = 0: \quad \mathcal{Y}(\mathbb{M}) &= \left[ {}_2F_1 \left( \left\{ \begin{array}{c} -1/6 \\ 1/3 \end{array} \right\}, 1, \frac{4\mathbb{M}^2}{\pi^2} \right) + \frac{4\mathbb{M}}{3\pi^2} {}_3F_2 \left( \left\{ \begin{array}{c} 1/3 \\ 5/6 \\ 1 \end{array} \right\}, \left\{ \begin{array}{c} 3/2 \\ 3/2 \end{array} \right\}, \frac{4\mathbb{M}^2}{\pi^2} \right) \right]^{-1} \end{aligned}$$

and  ${}_2F_1$  and  ${}_3F_2$  are generalized hypergeometric functions (Abramowitz and Stegun, 1972).

Finally, an ODE governing evolution of  $\mathbb{M}$  with time is obtained from the 2nd expression in (26), recast as  $t\dot{\ell}/\ell = \mathbb{M}/(\gamma_k^2 \mathcal{M})$ , and upon substituting  $t\dot{\ell}/\ell = t\dot{V}/V + t\dot{\gamma}_k/\gamma_k$ , see (17) in the toughness scaling, and  $\gamma_k = \mathcal{Y}(\mathbb{M})$ , see (43),

$$\frac{t\dot{V}}{V} + \frac{d \ln \mathcal{Y}(\mathbb{M})}{d \ln t} = \frac{\mathbb{M}}{\mathcal{M}(t) \mathcal{Y}^2(\mathbb{M})} \quad (44)$$

where explicit dimensionless viscosity parameter  $\mathcal{M}(t)$  is given by the 2nd in (27). Further, it may prove convenient to reformulate this ODE using  $\mathcal{M}$  as the ‘time’ variable. Relating the log-derivatives,  $d \ln \mathcal{M}/d \ln t = 2t\dot{V}/V - 1$ , we have

$$\frac{t\dot{V}}{V} + \left(2 \frac{t\dot{V}}{V} - 1\right) \frac{d \ln \mathcal{Y}(\mathbb{M})}{d \ln \mathcal{M}} = \frac{\mathbb{M}}{\mathcal{M} \mathcal{Y}^2(\mathbb{M})} \quad (45)$$

Evidently, EofM in this form is particularly useful when injected fluid volume is a power-law of time, i.e. when  $\alpha = t\dot{V}/V = \text{const}$ , and solution  $\mathbb{M} = \mathbb{M}(\mathcal{M})$  of (45) depends on the single parameter - the fluid-volume-power-law-exponent  $\alpha$ . Once this ODE is solved, the approximate solution for the normalized half-length, (43), and opening, (41) when  $\alpha > 0$  and (42) when  $\alpha = 0$ , is complete.

## 5.2 Initial Conditions

Initial conditions at small fracture propagation time for either full numerical treatment of the problem (Appendix A) or in the approximate EofM approach discussed in the above normally correspond to small- $\mathcal{M}$  asymptote for the ‘fast’,  $\alpha = t\dot{V}/V > 1/2$ , and large- $\mathcal{M}$  asymptote for the ‘slow’,  $\alpha < 1/2$ , injection.

Small- $\mathcal{M}$  asymptotic solution in the toughness-scaling is given by (31), which we re-write here retaining the leading-order term only for simplicity

$$\mathcal{M} \ll 1: \quad \mathbb{M} \approx \alpha\mathcal{M}, \quad \gamma_k \approx 1, \quad \Omega_k \approx 1 \quad (46)$$

Large- $\mathcal{M}$  asymptotic solution corresponds to the zero-toughness solution given in the viscosity scaling by (40). Converting the latter to the toughness-scaling

$$\mathcal{M} \gg 1: \quad \mathbb{M} = \left( \frac{(3\alpha + 1)\gamma_m^2}{5} \right)^{3/5} \mathcal{M}^{3/5}, \quad \gamma_k = \mathbb{M}^{-1/3}\gamma_m, \quad \Omega_k = \mathbb{M}^{1/3}\Omega_m \quad (47)$$

where  $\gamma_m = \gamma_m(\alpha)$  and  $\Omega_m = \Omega_m(\xi; \alpha)$  is the zero-toughness solution (40).

## 5.3 Solution for Power-Law Fluid Injection

This section presents regime-transient solution for continuous power-law injection  $V \propto t^\alpha$  with non-zero material toughness. Zero-viscosity (toughness-dominated regime) and zero-toughness (viscosity-dominated regime) end-members of this solution have been given in Sections 4.1 and 4.2.

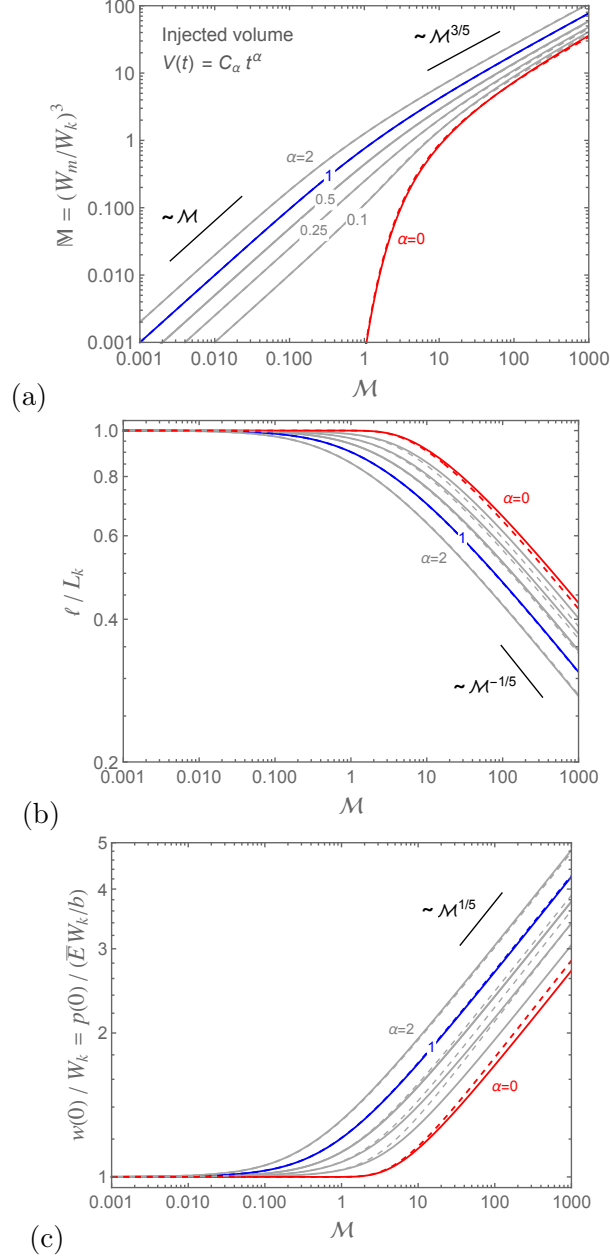


Figure 5: Power-law injection solution in the toughness scaling. Equation-of-Motion (dashed) and the fully numerical Method-of-Lines (solid) solutions for hydraulic fracture propagation driven by a power-law injection  $V(t) = Ct^\alpha$  for various values of  $\alpha$ : 0 (constant volume), 0.1, 0.25, 0.5 (constant injection pressure), 1 (constant rate of injection), and 2. **(a)** Implicit dimensionless viscosity parameter  $\bar{M} \propto \ell \ell$  evolution with the explicit dimensionless viscosity parameter  $\mathcal{M}(t) \propto V^2(t)/t$ . **(b,c)** Corresponding evolution of the normalized crack half-length  $\ell/L_k(t)$  and opening/net-pressure at the inlet  $w(0)/W_k = p(0)/(\bar{E}W_k/b)$  with  $\mathcal{M}(t)$ . Dependence of the solution on time follows from that of the scales,  $W_k = \bar{K}\sqrt{b}/\bar{E}$  and  $L_k(t) = V(t)/(2bW_k)$ , and of the evolution parameter  $\mathcal{M}(t) = (3\bar{\mu}\bar{E}^4/4\bar{K}^5b^{7/2})(V^2(t)/t)$ , as further explored in Fig. 6.

Fig. 5 shows the dimensionless solution in the *toughness-scaling* for various values of injection power-law  $\alpha$ , namely the evolution of dimensionless implicit viscosity parameter  $\mathbb{M}$ , the normalized fracture half-length, and opening at the inlet with explicit, time-dependent dimensionless viscosity parameter  $\mathcal{M}(t)$ . The solution corresponds to the transition from the toughness- to viscosity- dominated regime of propagation with increasing value of  $\mathcal{M}$ , with corresponding asymptotic solutions given by the zero-viscosity and zero-toughness solutions discussed earlier, respectively. Given different sense of time-dependence of  $\mathcal{M}$  depending on the power-law  $\alpha$ ,  $\mathcal{M} \propto t^{2\alpha-1}$ , the aforementioned regime transition in time is from the toughness- to the viscosity- regime for ‘fast’ injections  $\alpha > 1/2$  and is reversed for ‘slow’ injections  $0 \leq \alpha < 1/2$ . Change of the archetype of the transient solution takes place for an injection with  $\alpha = 1/2$ , which correspond to injection with constant injection pressure at the crack inlet and corresponding self-similar solution ( $\mathcal{M}$  is time-independent constant). Thus, ‘fast’ injections leading to toughness-to-viscosity regime transition in time are characterized by increasing fluid pressure (and therefore crack opening) at the inlet with time, while ‘slow’ injections leading to the viscosity-to-toughness transition correspond to decreasing injection pressure in time.

### Explicit time-dependence of the solution - transitional *MK* scaling

Given non-trivial time-dependence of both the evolution parameter  $\mathcal{M}(t)$  and lengthscale  $L_k(t)$  pertaining to the toughness-scaling of the solution in Fig. 5, we seek to rescale into a different, time-independent scaling in order to illustrate the explicit dependence of the solution for the crack opening  $w$  (net fluid pressure  $p = E' w/b$ ) and the crack half-length  $\ell$  on time.

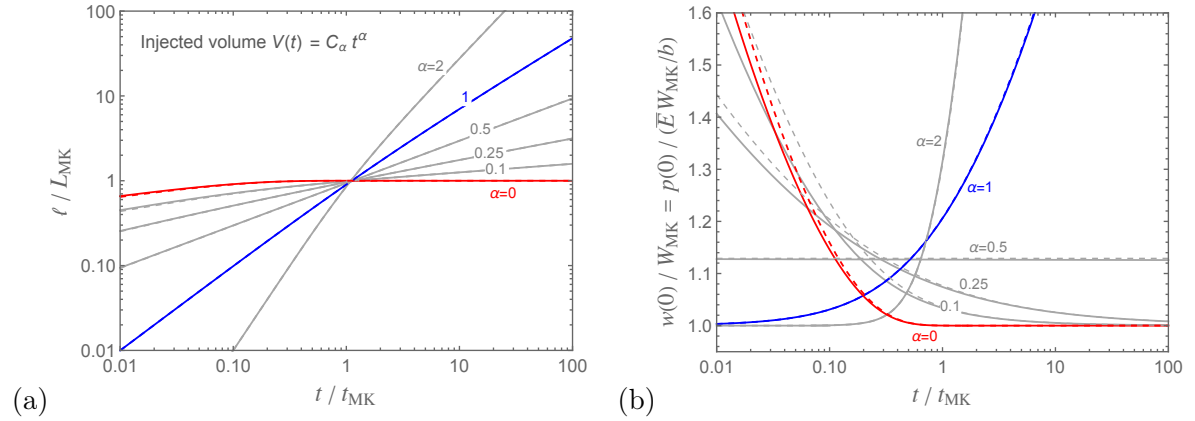


Figure 6: Power-law injection solution in the transitional *MK* scaling (explicit time dependence). Solution for the crack half-length and opening/net-pressure of Fig. 5(b-c) re-scaled using the time-independent scales,  $\ell/L_{MK}(\alpha)$  and  $w(0)/W_{MK} = p(0)/(E W_{MK}/h)$ , and shown as a function of normalized time  $\tau = t/t_{MK}(\alpha)$ . The transitional scales are  $W_{MK} = W_k$  and  $t_{MK}(\alpha)$ ,  $L_{MK}(\alpha)$  given by (48), while evolution parameter of Fig. 5 is  $\mathcal{M}(t) = \tau^{2\alpha-1}$ . Note that ‘fast’  $\alpha > 0.5$  injection corresponds to the fracture evolution in time from the toughness to the viscosity-dominated regime, while the opposite is true for ‘slow’  $\alpha < 0.5$  injection, including the constant-volume case  $\alpha = 0$ .

Let us define transitional timescale as the time  $t = t_{MK}$  when the viscosity and toughness

crack aperture scales assume the same value, further denoted as transitional opening scale  $W_{MK}$ :

$$W_{MK} = \bar{W}_m(t_{MK}) = W_k \quad \Rightarrow \quad \frac{V^2(t_{MK})}{t_{MK}} = \frac{4}{3} \frac{\bar{K}^5 b^{7/2}}{\bar{\mu} \bar{E}^4}$$

By their definitions, the dimensionless, time-dependent viscosity and toughness parameters attain value of unity at  $t = t_{MK}$ , i.e.  $\mathcal{M}(t_{MK}) = \mathcal{K}(t_{MK}) = 1$ .

Corresponding transitional crack lengthscale is then defined by

$$L_{MK} \equiv \bar{L}_m(t_{MK}) = L_k(t_{MK})$$

Intuitively,  $t_{MK}$ ,  $L_{MK}$ , and  $W_{MK}$  should scale the time, crack length and opening when the transition between the viscosity and toughness dominated regimes takes place.

For power-law injection  $V(t) = C_\alpha t^\alpha$  (such that  $C_0 = V_0$  for fixed volume injection, and  $C_1 = Q_o$  for constant rate injection) we have

$$t_{MK} = \left( \frac{3}{4} \frac{\bar{\mu} \bar{E}^4 C_\alpha^2}{\bar{K}^5 b^{7/2}} \right)^{1/(1-2\alpha)}, \quad L_{MK} = \left( \frac{3^\alpha}{2} \frac{\bar{\mu}^\alpha \bar{E}^{1+2\alpha} C_\alpha}{\bar{K}^{1+3\alpha} b^{(3+\alpha)/2}} \right)^{1/(1-2\alpha)} \quad (48)$$

For example, taking the fixed volume ( $\alpha = 0$ ,  $C_0 = V_0$ ) and fixed injection rate ( $\alpha = 1$ ,  $C_1 = Q_0$ ) cases, the corresponding expressions for the time and lengthscales evaluate to:

$$\alpha = 0: \quad t_{MK} = \frac{3}{4} \frac{\bar{\mu} \bar{E}^4 V_0^2}{\bar{K}^5 b^{7/2}}, \quad L_{MK} = \frac{\bar{E} V_0}{2 \bar{K} b^{3/2}} \quad (49)$$

$$\alpha = 1: \quad t_{MK} = \frac{4}{3} \frac{\bar{K}^5 b^{7/2}}{\bar{\mu} \bar{E}^4 Q_0^2}, \quad L_{MK} = \frac{2}{3} \frac{\bar{K}^4 b^2}{\bar{\mu} \bar{E}^3 Q_0} \quad (50)$$

Corresponding solution conversion relations between the toughness  $k$  and transitional  $MK$  scalings follow in the form of power laws of the normalized time  $t/t_{MK}$ ,

$$\mathcal{M} = \mathcal{K}^{-5} = \left( \frac{t}{t_{MK}} \right)^{2\alpha-1}, \quad \frac{\gamma_{MK}}{\gamma_k} = \frac{L_k}{L_{MK}} = \left( \frac{t}{t_{MK}} \right)^\alpha, \quad \frac{\Omega_{MK}}{\Omega_k} = \frac{W_k}{W_{MK}} = 1 \quad (51)$$

Transient solutions for power-law injection rescaled to the  $MK$  scaling, and, therefore, showing explicit dependence of the crack length and opening on time, are shown on Fig. 6. Particularly for the opening, Fig. 6b clearly shows the increasing / diminishing opening with continuing crack propagation for ‘faster’  $\alpha > 1/2$  and ‘slower’  $\alpha < 1/2$  injection power-laws  $V \propto t^\alpha$ , respectively.

At  $\alpha = 1/2$ , the transitional scaling is singular, i.e. transition time  $t_{MK}$  and length  $L_{MK}$  scales are clearly either zero or infinite, see (48). In this case,  $\mathcal{M}$  is time-invariant constant, reflecting the stationarity (absence of transition) of the fracture propagation regime and the self-similarity of the corresponding solution. As the result, the solution in transitional scaling for  $\alpha = 1/2$  lacks clear meaning, and the reader is referred to the solution in a non-singular scaling, such as the toughness-scaling, in Fig. 5.

## Accuracy of EoM solution

Accuracy of the EofM approximate solutions can be gaged from Figs. 5-6, which contrast the former, shown by dashed lines, with the method-of-lines numerical solutions shown by solid lines and characterized by the superior accuracy (sub 0.1% error, cf. Appendix B.1). EofM accuracy is seen to depend on the injection power-law  $\alpha$ . The relative error of approximation of the crack half-length and opening generally does not exceed few percent (and is particularly good for the constant injection rate solution for which the error upper bound corresponds to that of the zero-toughness solution limit discussed earlier, i.e. <1% for length and <5% for the opening). More details on the EofM errors and their estimation are given in Appendix B.2 and Fig. B.4.

## 5.4 Solution for Fluid Injection Followed by Shut-in

In the shut-in problem, the fracture is first advanced by fluid injection over a period of time, followed by the shut-in and subsequent propagation with the fixed fracture volume. The fixed-volume fracture solution of Section 5.3 considers fracture propagation due to an *instantaneous* injection of a finite volume of fluid. In the context of the shut-in problem, this asymptotic solution is therefore expected to provide the large-time, post-shut-in asymptote, when the details of the fracture evolution during the pre-shut-in period become inconsequential. This asymptotic solution, as shown on Fig. 6 in red ( $\alpha = 0$ ), starts out of the viscosity-dominated regime and ends up in the toughness-dominated regime.

Full solution to the shut-in problem on a *finite* shut-in timescale considered here corresponds to an injection at *constant rate* which persists over finite duration  $t < t_0$ , followed by the shut-in for  $t \geq t_0$ . Corresponding evolution of the dimensionless viscosity is non-monotonic, increasing from zero (toughness-dominated regime) at early time to the maximum value  $\mathcal{M}_0 = \mathcal{M}(t_0)$  at the shut-in, and then decreasing asymptotically back to zero (fracture arrest) at large time. Solution *prior to the shut-in*,  $t < t_0$ , has been given in Section 5.3 using both simplified EoM and the fully-numerical method-of-lines approaches and shown on Fig. 6 ( $\alpha = 1$ ). The *post-shut-in* solution,  $t \geq t_0$ , is obtained here using the same two approaches with  $t\dot{V}/V$  set to zero<sup>3</sup> and the ‘initial’ conditions at the shut-in  $t = t_0$  are those of solution continuity, i.e. given by the aforementioned injection solution up to that moment.

Normalized solution for the implicit viscosity  $\mathbb{M} \propto \ell \dot{\ell}$ , crack length, and inlet opening / net-pressure in the toughness scaling is shown on Fig. 7 for various values of the shut-in time, as quantified by the corresponding values of dimensionless viscosity parameter  $\mathcal{M}_0 = \mathcal{M}(t_0)$ . The injection part of the solution, shown in blue, evolves, as previously discussed, from the toughness- towards the viscosity-dominated regime with  $\mathcal{M}(t)$  increasing with time, while the post-shut-in solution, shown in red, signifies a reverse regime transition with  $\mathcal{M}(t)$  now decreasing with time, back towards toughness-dominated regime (asymptotic arrested fracture state).

We note with regard to the EofM solution that the approximation for non-dimensional crack length  $\gamma_k \approx \mathcal{Y}(\mathbb{M})$  in the EofM framework is distinct for injection and post-shut-in (cf. (43)). Thus, continuity of EofM solution at  $t = t_0$  can only be enforced for *either* fracture length  $\gamma_k$  *or* dynamic non-dimensional parameter  $\mathbb{M}$  (proportional to fracture length and its time rate). EofM post-shut-in solutions presented here use the fracture-length continuity and

---

<sup>3</sup>see EofM (45) and equation (A.5) in Appendix A, respectively.

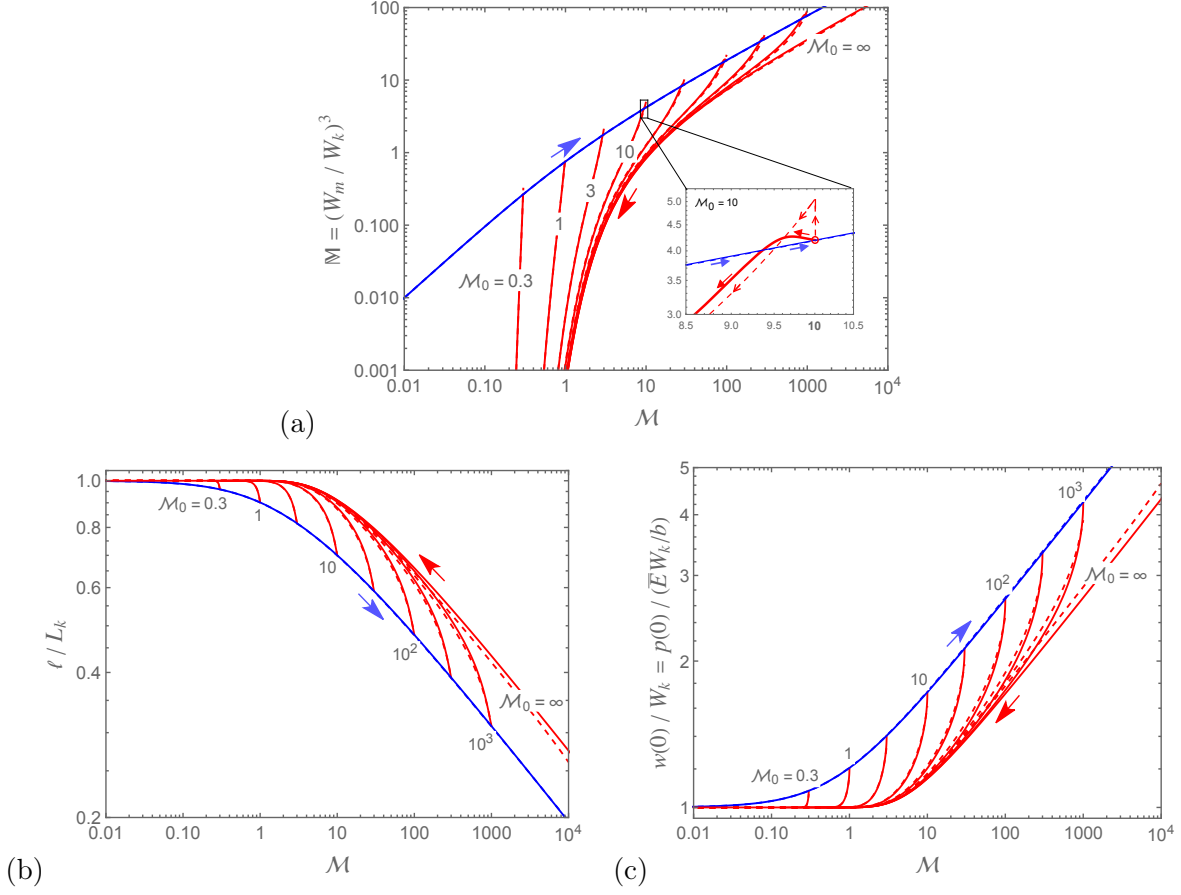


Figure 7: Shut-in problem. Equation-of-Motion (dashed) and the numerical Method-of-Lines (solid) solutions for the hydraulic fracture propagation driven by *injection* at constant rate  $V(t < t_0) = Q_0 t$  (blue) followed by *shut-in*  $V(t \geq t_0) = V_0 = Q_0 t_0$  (red) for various values of the shut-in time  $t_0$ , as correspond to the values of dimensionless viscosity parameter  $\mathcal{M}_0 = \mathcal{M}(t_0) = (3\bar{\mu}\bar{E}^4/4\bar{K}^5 b^{7/2})(V_0^2/t_0) = 0.3, 1, \dots, 300, 1000$ . **(a)** Implicit (crack-propagation-dependent) dimensionless viscosity parameter  $\mathbb{M} \propto \ell \dot{\ell}$  evolution with the explicit dimensionless viscosity parameter  $\mathcal{M}(t) \propto V^2(t)/t$ . **(b,c)** Corresponding evolution of the normalized crack half-length  $\ell/L_k(t)$  and opening/net-pressure at the inlet  $w(0)/W_k = p(0)/(\bar{E}W_k/b)$  with  $\mathcal{M}(t)$ . Dependence of the solution on time follows from that of the scales,  $W_k = \bar{K}\sqrt{b/\bar{E}}$  and  $L_k(t) = V(t)/(2bW_k)$ , and of the evolution parameter  $\mathcal{M}(t) = (3\bar{\mu}\bar{E}^4/4\bar{K}^5 b^{7/2})(V^2(t)/t)$ , as further explored in Fig. 8. The sense of time-evolution of  $\mathcal{M}(t)$  - increasing prior to the shut-in and decreasing post the shut-in - is indicated by arrows. The injection solution (blue) and the large-shut-in-time asymptote (red,  $\mathcal{M}_0 = \infty$ ) correspond to the power-law  $\alpha = 1$  (constant-volume-rate) and  $\alpha = 0$  (constant-volume) solutions in Fig. 5, respectively. Inset in (a) zooms into the evolution of the solution with  $\mathcal{M}_0 = 10$  near the shut-in instant.

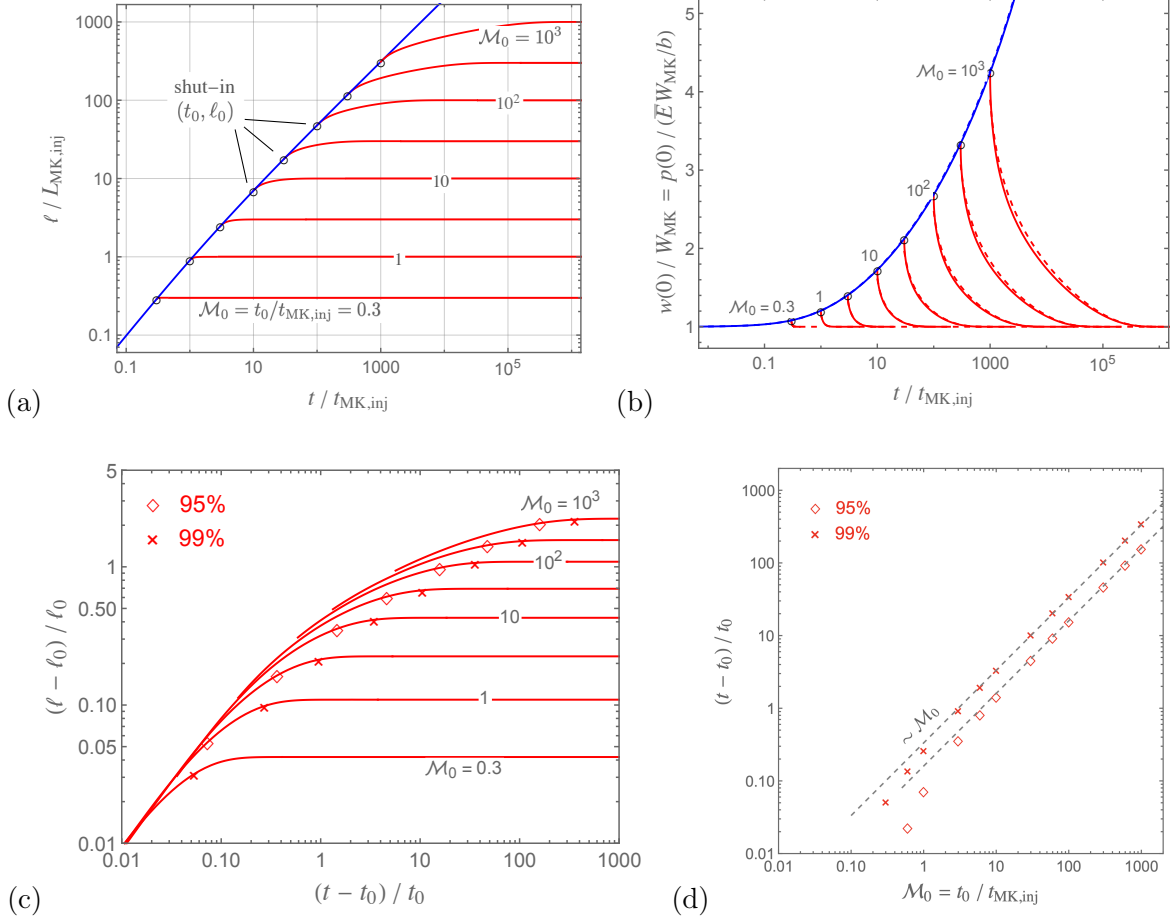


Figure 8: Shut-in problem. Solution for (a) crack half-length and (b) opening/net-pressure of Fig. 7(b-c) re-scaled using the time-independent scales,  $\ell / L_{MK, inj}$  and  $w(0) / W_{MK}$ , and shown as a function of scaled time  $\tau = t / t_{MK, inj}$ , where ‘inj’ indicates injection ( $\alpha = 1$ ) transitional scale (i.e.  $t_{MK, inj} = t_{MK}(\alpha = 1)$  given by (50)). (c) Post-shut-in crack growth,  $\ell - \ell_0$  vs.  $t - t_0$ , normalized by the shut-in values,  $\ell_0$  and  $t_0$ . Symbols marks the states corresponding to 95% and 99% of the terminal fracture length  $\ell_{max} = L_{k, V=V_0} = V_0 / (2bW_k)$ . (d) Normalized post-shut-in time  $(t - t_0) / t_0$  at 95% and 99% of the terminal fracture length from (c) shown vs. the normalized shut-in time  $\mathcal{M}_0 = t_0 / t_{MK, inj}$ . Dashed lines show a linear approximation for large-enough shut-in time.

thus, expectedly, have a discontinuity at  $t = t_0$  in the fracture speed, as well as, in the crack opening, the latter owing to the two distinct approximations for the opening during injection and post-shut-in, respectively, in the EofM approach. The inset in Fig. 7a zooms-in to show the discontinuity of  $\mathbb{M} \propto \ell \dot{\ell}$  in the EofM solution (dashed) compared to the continuity of the method-of-lines solution.

Given the changing nature the time-dependence of  $\mathcal{M} \propto V^2(t)/t$  and toughness lengthscale  $L_k \propto V(t)$ , and the different nature of this time-dependence pre- and post- shut-in, we show the shut-in solution rescaled to the time-independent, injection transitional scaling in Fig. 8 (i.e. using scales  $t_{\text{MK},\text{inj}}$ ,  $L_{\text{MK},\text{inj}}$ , and  $W_{\text{MK},\text{inj}} = W_k$  where the index ‘inj’ indicates injection-scaling (50)). Specifically, Fig. 8a-b show the evolution in time of the crack half-length and inlet opening / net-pressure. We observe the post-shut-in continued growth of the hydraulic fracture towards the terminal, toughness-dominated state, with the extent of this growth an increasing function of the dimensionless viscosity at the shut-in  $\mathcal{M}_0$ , which can also be understood in terms of the increasing shut-in time  $t_0$  and volume  $V_0$ . In other words, the further away is the fracture propagation regime from being toughness-dominated at the shut-in of the injection, the longer is the subsequent post-shut-in evolution towards the fixed-volume toughness-dominated crack. This thesis is further explored in Fig. 8c showing the extent of the post-shut-in crack growth (relative to the shut-in crack length) vs. the post-shut-in duration (relative to the injection duration). The symbols indicate the fracture within 1% or 5% of the terminal length. Since the shut-in crack length  $\ell_0$  is increasing with the increased injection duration  $t_0$  (see the injection solution of Fig. 8a shown in blue), the post-shut-in crack growth  $\ell - \ell_0$  is increasing faster than linearly with  $\ell_0$ , Fig. 8c. Corresponding normalized post-shut-in time  $(t - t_0)/t_0$  for the fracture to reach within 1% or 5% of its final extent is shown as a function of the normalized shut-in time  $\mathcal{M}_0 = t_0/t_{\text{MK},\text{inj}}$  on Fig. 8d. Apart from the cases corresponding to small shut-in time (when the pre-shut-in fracture propagates in/near the toughness-dominated regime,  $\mathcal{M}_0 < 1$ ), the Fig. suggests a linear scaling for the normalized post-shut-in growth time  $(t - t_0)/t_0$  with  $t_0$  shown by dotted lines. This translates to a quadratic dependence for the dimensional post-shut-in time, e.g. the post-shut-in time to reach 95% of the terminal length is  $t_{95\%} - t_0 \approx 0.16 \times t_0^2/t_{\text{MK},\text{inj}}$  (Fig. 8d).

Finally, Fig. 8b tracks the evolution of the inlet opening / net-pressure with time, illustrating the inflation of the crack at the inlet during the injection period, with subsequent deflation post-shut-in towards the final values  $W = W_k$  and  $p = P_k = \bar{E}W_k/b$ , respectively. Since the fracture volume remains fixed post-shut-in, the latter inlet deflation corresponds to the continued incremental crack growth and redistribution of fluid within the crack, away from the inlet.

## 6 Discussion and Conclusions

The original PKN model of elongated hydraulic fracture propagation (Perkins and Kern, 1961; Nordgren, 1972) neglects the effect of rock toughness, in favor of the dissipation in the viscous fluid flow inside the fracture. In other words, energy dissipation in breaking the rock is assumed negligible compared to that in the viscous fluid in the PKN elongated fracturing. Energy considerations for hydraulic fractures of other geometries (radial, plane-strain) have also seem to indicate that the rock toughness, if constrained by the lab-scale measurements, can be neglected in industrial hydraulic fracturing treatments, for the representative values of

the fracturing fluid viscosity, injection rate and fracture scale (e.g., Garagash, 2009; Garagash et al., 2011; Detournay, 2016).

The extension of the PKN model to account for the rock fracture toughness (Sarvaramini and Garagash, 2015; Chuprakov et al., 2017; Dontsov, 2022a) and solutions thereof developed in this work allow to evaluate the effect of rock toughness on different stages of HF propagation, during injection and shut-in. In doing so, we can evaluate the effect of toughness assuming either (i) typical values measured in the laboratory, small-scale tests; or (ii) order(s) of magnitude larger, fracture-scale-dependent values inferred, albeit not without controversy, from observations.

Table 2: An example of the regime-transition time  $t_{MK}$  and length  $L_{MK}$  scales for a typical slick-water hydraulic fracturing treatment: during injection (regime transition  $K \rightarrow M$ ) and during the shut-in (transition towards the  $K$ -regime of the terminal fracture) evaluated for three distinct realizations of the fracture energy scaling with fracture height  $G_c \propto b^\chi$ , Eq. (1):  $\chi = 0$  (scale-invariant), 0.5 (sub-linear), 1 (linear). The values of the non-dimensional viscosity (regime parameter)  $\mathcal{M}_0 = \mathcal{M}(t_0)$  and fracture half-length  $\ell(t_0)$  at the end of injection are also given. Parameter set for a field elongated fracture (Fig. 1b,c) was used: fracture height  $2b \approx 0.1$  km, injection rate,  $Q \approx 100$  L/s ( $t < t_0 \approx 2.8$  hr,  $2V(t) < 2V_o \approx 10^3$  m<sup>3</sup>) and  $Q = 0$  ( $t \geq t_0$ ), fluid viscosity of fracturing gel  $\mu = 150$  cP, and the values of the rock parameters,  $E' = 30$  GPa and  $K_{Ic,0} = 1$  MPa $\sqrt{m}$ , corresponding to small-scale ( $2b_0 \sim 0.1$ m) laboratory measurements on a reservoir sandstone (e.g. Chandler et al., 2016).

Frac. energy scaling $G_c \propto b^\chi$	Frac. toughness MPa $\sqrt{m}$	Injection ( $K \rightarrow M$ )		Shut-in ( $\rightarrow K$ )			
		$t_{MK}$ , hr	$L_{MK}$ , km	$\mathcal{M}(t_0)$	$\ell(t_0)$ , km	$t_{MK}$ , hr	$L_{MK} = \ell(\infty)$ , km
$\chi = 0$ (scale-invariant)	1	$\approx 0$	$\approx 0$	$\sim 10^6$	0.6	$\sim 10^6$	8.5
$\chi = 0.5$ (sub-linear)	5.6	0.005	0.005	300	0.6	400	1.5
$\chi = 1$ (linear)	32	27	5	0.05	0.27	0.07	0.27

Effects of toughness and its scaling with the fracture height on the dominant propagation regime of a hydraulic fracture are illustrated in Table 2 for the values of problem parameters representative of a gel (high-viscosity) fracturing treatment in Cartage Cotton Valley gas reservoir (Rutledge et al., 2004; Mayerhofer et al., 2000).. The dominant regimes can be ascertained by comparing the regime-transition time (and length) scales to the injection time  $t_0 \approx 2.8$  hr and fracture length  $\ell(t_0)$ , respectively.

Assuming scale-invariance ( $\chi = 0$ ) of the fracture toughness (i.e. the field fracture toughness is given by the small-scale laboratory value  $K_{Ic} = K_{Ic,0} = 1$  MPa $\sqrt{m}$ ), we observe that the injection stage is viscosity-dominated, i.e. the time  $t_{MK}$  to transition from the ‘early-time’ toughness ( $K$ ) to the ‘large-time’ viscosity ( $M$ ) dominated regime is vanishingly small. Corresponding non-dimensional viscosity evaluated at the end of injection is exceedingly large, underlining irrelevance of rock toughness during the injection stage for the considered case. Consequently, the post shut-in propagation from the at-shut-in  $M$  to the eventual  $K$  regime would occur over exceedingly large, impractical timescale  $\sim 10^6$  hr, with the corresponding forecasted post-shut-in fracture growth from 0.6 km to 8.5 km for the half-length. The fracturing fluid leak-off is expected to become dominant over large post-shut-in time (Dontsov, 2022a), which would effectively curtail the growth predicted here by the zero-leak-off model. However, even assuming the leak-off mediated final fracture half-length approximately equal to that at the shut-in, the theoretical prediction for the latter 0.6 km is unrealistic when con-

trasted to the final fracture half-length value  $\ell_{\text{final}} \approx 0.4$  km inferred from observations (Fig. 1b,c).

A very different picture of the fracture evolution emerges for a scale-dependent fracture toughness. Considering the linear fracture energy scaling with height ( $\chi = 1$ ), the corresponding field fracture toughness in this example,  $K_{Ic} \approx 32$  MPa $\sqrt{\text{m}}$ , is more than an order of magnitude larger than the laboratory value, which leads to the toughness-dominated injection and post-shut-in propagation. Indeed, the time  $t_{\text{MK}}$  to transition from the ‘early-time’ toughness ( $K$ ) to the ‘large-time’ viscosity ( $M$ ) dominated regime during *injection* is exceedingly large in this case (much larger than the injection time period). This is further highlighted by very small value of the non-dimensional viscosity at the end of injection,  $\mathcal{M}(t_0) \approx 0.05$ , and negligible post-shut-in propagation over a very short post-shut-in transition timescale (0.07 hr). The final predicted fracture half-length 0.27 km is comparable to the observed 0.4 km (Fig. 1b,c).

Consequently, we surmise based on this typical field example that hydraulic fracture propagation is viscosity-dominated, and therefore adequately approximated by the zero-toughness solution (i.e. the original PKN model (Perkins and Kern, 1961; Nordgren, 1972)), when a typical laboratory (small-scale) fracture toughness value  $\sim 1$  MPa $\sqrt{\text{m}}$  is assumed. The opposite is true, i.e. the hydraulic fracture propagation is predicted to be toughness-dominated, and therefore adequately approximated by the zero-viscosity solution, if scale-dependence of the fracture toughness is invoked. This conclusion arrived at in the example of high-viscosity gel fluid fracturing will certainly hold for low-viscosity (e.g. ‘slick’ water) fracturing.

Examination of a larger well-constrained dataset for field hydraulic fracture and dikes and model inversion thereof is needed to further validate the scale dependence argument.

## References

- Abramowitz, M., Stegun, I. (Eds.), 1972. Handbook of Mathematical Functions with Formulas, Graphs, and Mathematical Tables. Dover Publications Inc., New York NY.
- Adachi, J., Siebrits, E., Peirce, A., Desroches, J., 2006. Computer simulation of hydraulic fractures. *Int. J. Rock Mech. Min. Sci.* 44, 739–757.
- Adachi, J.I., Detournay, E., Peirce, A.P., 2010. Analysis of the classical pseudo-3d model for hydraulic fracture with equilibrium height growth across stress barriers. *International Journal of Rock Mechanics and Mining Sciences* 47, 625–639.
- Adachi, J.I., Peirce, A.P., 2008. Asymptotic analysis of an elasticity equation for a finger-like hydraulic fracture. *J. Elast.* 90, 43–69. doi:10.1007/s10659-007-9122-4.
- Chandler, M.R., Meredith, P.G., Brantut, N., Crawford, B.R., 2016. Fracture toughness anisotropy in shale. *Journal of Geophysical Research: Solid Earth* 121, 1706–1729.
- Chuprakov, D., Izimov, R., Spesivtsev, P., 2017. Continued hydraulic fracture growth after well shut-in, in: 51st US Rock Mechanics/Geomechanics Symposium, OnePetro. pp. 1–17.
- Davis, T., Rivalta, E., Dahm, T., 2020. Critical fluid injection volumes for uncontrolled fracture ascent. *Geophys. Res. Lett.* doi:10.1029/2020GL087774.
- Delaney, P.T., Pollard, D.D., Ziony, J.I., McKee, E.H., 1986. Field relations between dikes and joints: Emplacement processes and paleostress analysis. *Journal of Geophysical Research: Solid Earth* 91, 4920–4938.
- Detournay, E., 2016. Mechanics of hydraulic fractures. *Annu. Rev. Fluid Mech.* 48. doi:10.1146/annurev-fluid-010814-014736.
- Dontsov, E., 2022a. Analysis of a constant height hydraulic fracture, in: Zhang, X., Wu, B., Yang, D., Bungler, A. (Eds.), *Mechanics of Hydraulic Fracturing: Experiment, Model, and Monitoring*. Wiley. chapter 11, pp. 127–139. doi:10.1002/9781119742487.ch11.
- Dontsov, E., 2022b. Analysis of a constant height hydraulic fracture driven by a power-law fluid. *Rock Mechanics Bulletin* 1, 100003.
- Dontsov, E., Peirce, A., 2016. Comparison of toughness propagation criteria for blade-like and pseudo-3d hydraulic fractures. *Engineering Fracture Mechanics* 160, 238–247.
- Dontsov, E.V., 2016. An approximate solution for a penny-shaped hydraulic fracture that accounts for fracture toughness, fluid viscosity and leak-off. *R. Soc. open sci.* 3, 160737. doi:10.1098/rsos.160737.
- Dontsov, E.V., 2017. An approximate solution for a plane strain hydraulic fracture that accounts for fracture toughness, fluid viscosity, and leak-off. *Int. J. Fracture* 205, 221–237. doi:10.1007/s10704-017-0192-4.

- Garagash, D., Germanovich, L., 2014. Gravity driven hydraulic fracture with finite breadth, in: Bajaj, A., Zavattieri, P., Koslowski, M., Siegmund, T. (Eds.), *Proceedings of the Society of Engineering Science 51st Annual Technical Meeting, October 1-3, 2014*, Purdue University Libraries Scholarly Publishing Services, West Lafayette.
- Garagash, D.I., 2006. Plane strain propagation of a fluid-driven fracture during injection and shut-in: Asymptotics of large toughness. *Engng. Frac. Mech.* 73, 456–481.
- Garagash, D.I., 2009. Scaling of physical processes in fluid-driven fracture: Perspective from the tip, in: Borodich, F. (Ed.), *IUTAM Symposium on Scaling in Solid Mechanics*, Springer. pp. 91–100.
- Garagash, D.I., 2019. Cohesive-zone effects in hydraulic fracture propagation. *J. Mech. Phys. Solids* 133. doi:10.1016/j.jmps.2019.103727.
- Garagash, D.I., 2022. Notes on hydraulic fracture mechanics. arXiv:2209.12008v1 .
- Garagash, D.I., Detournay, E., Adachi, J.I., 2011. Multiscale tip asymptotics in hydraulic fracture with leak-off. *J. Fluid Mech.* 669, 260–297. doi:10.1017/S002211201000501X.
- Garagash, D.I., Germanovich, L.N., 2022. Notes on propagation of 3d buoyant fluid-driven cracks. arXiv:2208.14629 .
- Hutchinson, J.W., Suo, Z., 1992. Mixed mode cracking in layered materials. *Adv. Appl. Mech.* 29, 63–191. Interface crack, mixed mode.
- Kemp, L.F., 1990. Study of Nordgren’s equation of hydraulic fracturing. *SPE Prod. Eng.* , 311–314.
- Kovalyshen, Y., Detournay, E., 2010. A reexamination of the classical pkn model of hydraulic fracture. *Transport in Porous Media* 81, 317–339. doi:10.1007/s11242-009-9403-4.
- Laubach, S., Monson, E., 1988. Coring-induced fractures: Indicators of hydraulic fracture propagation in a naturally fractured reservoir, in: *SPE Annual Technical Conference and Exhibition, OnePetro*. p. 18164.
- Lister, J.R., 1990. Buoyancy-driven fluid fracture: Similarity solutions for the horizontal and vertical propagation of fluid-filled cracks. *J. Fluid Mech.* 217, 213–239.
- Liu, D., Lecampion, B., 2022. Laboratory investigation of hydraulic fracture growth in zimbabwe gabbro. *Journal of Geophysical Research: Solid Earth* 127, e2022JB025678.
- Liu, D., Lecampion, B., Garagash, D.I., 2019. Propagation of a fluid-driven fracture with fracture length dependent apparent toughness. *Engng. Fract. Mech.* 220, 106616.
- Lopez, J.M., Schmittbuhl, J., 1998. Anomalous scaling of fracture surfaces. *Physical Review E* 57, 6405.
- Mayerhofer, M.J., Walker, R.N., Urbancic, T., Rutledge, J.T., 2000. East texas hydraulic fracture imaging project: Measuring hydraulic fracture growth of conventional sandfracs and waterfracs, in: *Proc. 2000 Soc. Petro. Eng. Annu. Tech. Conf., SPE*. pp. 1–12.

- Mishuris, G., Wrobel, M., Linkov, A., 2012. On modeling hydraulic fracture in proper variables: stiffness, accuracy, sensitivity. *International Journal of Engineering Science* 61, 10–23.
- Morel, S., Bouchaud, E., Schmittbuhl, J., Valentin, G., 2002. R-curve behavior and roughness development of fracture surfaces. *International Journal of Fracture* 114, 307–325.
- Möri, A., Lecampion, B., 2022. Three-dimensional buoyant hydraulic fractures: constant release from a point source. *J. Fluid Mech.* 950, A12. doi:10.1017/jfm.2022.800.
- Möri, A., Peruzzo, C., Garagash, D., Lecampion, B., 2024. How stress barriers and fracture toughness heterogeneities arrest buoyant hydraulic fractures. *Rock Mechanics and Rock Engineering* doi:10.1007/s00603-024-03936-0.
- Nara, Y., Morimoto, K., Hiroyoshi, N., Yoneda, T., Kaneko, K., Benson, P.M., 2012. Influence of relative humidity on fracture toughness of rock: implications for subcritical crack growth. *International Journal of Solids and Structures* 49, 2471–2481.
- Noël, C., Baud, P., Violay, M., 2021. Effect of water on sandstone’s fracture toughness and frictional parameters: Brittle strength constraints. *International Journal of Rock Mechanics and Mining Sciences* 147, 104916.
- Nolte, K.G., 1991. Fracturing-pressure analysis for nonideal behavior (SPE 20704). *J. Pet. Tech.* 43, 210–218.
- Nordgren, R.P., 1972. Propagation of vertical hydraulic fractures. *J. Pet. Tech.* 253, 306–314. (SPE 3009).
- Perkins, T.K., Kern, L.R., 1961. Widths of hydraulic fractures. *J. Pet. Tech., Trans. AIME* 222, 937–949.
- Peruzzo, C., Lecampion, B., 2024. How contained hydraulic fractures emerge from layers of alternating fracture toughness, in: 85th EAGE Annual Conference & Exhibition (including the Workshop Programme), European Association of Geoscientists & Engineers. pp. 1–5.
- Pollard, D.D., Aydin, A., 1988. Progress in understanding joints over the last century. *Geol. Soc. Am. Bull.* 100, 1181–1204.
- Rivalta, E., Taisne, B., Bungler, A., Katz, R., 2015. A review of mechanical models of dike propagation: Schools of thought, results and future directions. *Tectonophysics* 638, 1 – 42. URL: <http://www.sciencedirect.com/science/article/pii/S0040195114005174>, doi:<https://doi.org/10.1016/j.tecto.2014.10.003>.
- Rubin, A., Pollard, D., 1987. Origins of blade-like dikes in volcanic rift zones. *US Geological Survey Professional Paper* 1350, 1449–1470.
- Rutledge, J.T., Phillips, W.S., Mayerhofer, M.J., 2004. Faulting induced by forced fluid injection and fluid flow forced by faulting: An interpretation of hydraulic-fracture microseismicity, Carthage Cotton Valley gas field, Texas. *Bull. Seismol. Soc. Am.* 94, 1817–1830.
- Sarvaramini, E., Garagash, D.I., 2015. Breakdown of a pressurized finger-like crack in a permeable rock. *J. Appl. Mech.* 82, 061006.

- Schmidt, R., Huddle, C., 1977. Effect of confining pressure on fracture toughness of indiana limestone, in: *International Journal of Rock Mechanics and Mining Sciences & Geomechanics Abstracts*, Elsevier. pp. 289–293.
- Scholz, C.H., 2010. A note on the scaling relations for opening mode fractures in rock. *J. Struct. Geol.* 32, 1485–1487.
- Shlyapobersky, J., 1985. Energy analysis of hydraulic fracturing, in: *ARMA US Rock Mechanics/Geomechanics Symposium*, ARMA. pp. ARMA–85.
- Townsend, M.R., Pollard, D.D., Smith, R.P., 2017. Mechanical models for dikes: A third school of thought. *Tectonophysics* 703, 98–118.
- Warpinski, N., Branagan, P., Peterson, R., Wolhart, S., 1998. An interpretation of m-site hydraulic fracture diagnostic results, in: *SPE Rocky Mountain Petroleum Technology Conference/Low-Permeability Reservoirs Symposium*, SPE. pp. SPE–39950.
- Warpinski, N., Lorenz, J., Branagan, P., Myal, F., Gall, B., 1993. Examination of a cored hydraulic fracture in a deep gas well. *SPE Production & Facilities* 8, 150–158.
- Weng, H., Ampuero, J.P., 2019. The dynamics of elongated earthquake ruptures. *Journal of Geophysical Research: Solid Earth* 124, 8584–8610.
- Wrobel, M., Mishuris, G., 2015. Hydraulic fracture revisited: Particle velocity based simulation. *Int. J. Eng. Sci.* 94, 23–58.

## A Numerical Method-of-Lines Solution

In this Appendix we provide a method-of-line numerical solution method for a PKN fracture propagation. We solve the problem in the *toughness scaling*, specifically for the normalized opening  $\Omega$  as a function of normalized coordinate  $\xi$  and time  $t$  (or alternatively dimensionless viscosity  $\mathcal{M}(t)$ ). We approximate the cube of the opening  $\Omega^3(t, \xi)$  in space by piecewise linear distribution<sup>4</sup> defined by the values of the opening  $\Omega_i(t) = \Omega(t, \xi_i)$  at the uniformly spaced set of  $n + 1$  nodes  $\xi_i = i/n$  with  $i = 0, \dots, n$ .

Boundary conditions for the crack opening and fluid velocity at the crack tip dictate, respectively,

$$\Omega_n = 1, \quad \mathbb{M} = -\frac{\partial \Omega^3}{\partial \xi} \Big|_{\xi=1} \approx -\frac{3\Omega_n^3 - 4\Omega_{n-1}^3 + \Omega_{n-2}^3}{2/n} \quad (\text{A.1})$$

Carrying out the crack volume integral using the aforementioned piecewise linear approximation for  $\Omega^3$ , the global continuity yields

$$\frac{1}{\gamma} \approx \frac{3}{4/n} \sum_{i=0}^{n-1} \frac{\Omega_{i+1}^4 - \Omega_i^4}{\Omega_{i+1}^3 - \Omega_i^3} \quad (\text{A.2})$$

Alternatively, an inlet boundary condition can be used in place of the global continuity, as follows from (18), substituting  $t\dot{\ell}/\ell = \mathbb{M}/(\mathcal{M}\gamma^2)$ , and simplifying

$$\frac{t\dot{V}}{V} \mathcal{M}\gamma = -\frac{3}{4} \frac{\partial \Omega^4}{\partial \xi} \Big|_{\xi=0} \approx \frac{3}{4} \frac{3\Omega_0^4 - 4\Omega_1^4 + \Omega_2^4}{2/n} \quad (\text{A.3})$$

Combining local continuity (15) with the Poiseuille law, 1st in (20), and substituting  $t\dot{\ell}/\ell = \mathbb{M}/(\mathcal{M}\gamma^2)$  yields upon rearranging the double-derivative term:

$$t\dot{\Omega} - \frac{\mathbb{M}}{\mathcal{M}\gamma^2} \left( \xi \frac{\partial \Omega}{\partial \xi} + \frac{3}{4\mathbb{M}} \frac{\partial^2 \Omega^4}{\partial \xi^2} \right) = 0$$

Which approximation over the internal  $n - 1$  nodes using 2nd order central finite differences for spatial derivatives yields  $n - 1$  ODEs

$$\frac{d\Omega_i}{d \ln t} - \frac{\mathbb{M}}{\mathcal{M}\gamma^2} \left( \xi_i \frac{\Omega_{i+1} - \Omega_{i-1}}{2/n} + \frac{3}{4\mathbb{M}} \frac{\Omega_{i+1}^4 - 2\Omega_i^4 + \Omega_{i-1}^4}{1/n^2} \right) = 0 \quad (i = 1, \dots, n - 1) \quad (\text{A.4})$$

The closing ODE is rendered by plugging  $t\dot{\ell}/\ell = t\dot{V}/V + t\dot{\gamma}/\gamma$  into relation  $t\dot{\ell}/\ell = \mathbb{M}/(\mathcal{M}\gamma^2)$

$$\frac{t\dot{V}}{V} + \frac{d \ln \gamma}{d \ln t} = \frac{\mathbb{M}}{\mathcal{M}\gamma^2} \quad (\text{A.5})$$

Equations (A.4) and (A.5) provide a system of  $n$  ODEs to solve for the evolution in time of  $n$  unknowns  $\Omega_0, \dots, \Omega_{n-1}$  in lieu of the known  $\Omega_n = 1$  and the above expressions for  $\mathbb{M}$ , 2nd in (A.1), and  $\gamma$ , either (A.2) or (A.3).

Once again we can choose to use dimensionless viscosity  $\mathcal{M}$  as a 'time' by exchanging logarithmic time derivative in above for (45). As discussed in the main text, this is particularly convenient when injected fluid volume is a given power law of time, i.e.  $t\dot{V}/V = \alpha = \text{const}$ .

<sup>4</sup>Linear approximation for  $\Omega^3$  is asymptotically correct at the tip

The initial conditions for an injection problem with  $\alpha > 1/2$  correspond to the toughness-dominated conditions and are prescribed at some small initial value of  $\mathcal{M} = \mathcal{M}_{\text{ini}} \ll 1$  by the small-viscosity solution (46). In the case when  $\alpha < 1/2$ , the initial conditions corresponds to the viscosity-dominated conditions, and zero-toughness solution, expressed in the toughness scaling, (47), at some large  $\mathcal{M} = \mathcal{M}_{\text{ini}} \gg 1$  is used to initialize the solution.

The shut-in part of the crack evolution for  $t \geq t_0$  ( $\mathcal{M} \leq \mathcal{M}_0$ ) is solved for using the same framework with  $t\dot{V}/V$  set to zero and 'initial' conditions at  $t = t_0$  given by the injection solution up to that moment.

Numerical solutions presented in the main text and figures use the global continuity approximation for  $\gamma$ , (A.2), and are carried using  $n = 50$  spatial elements. Numerical error and convergence are discussed in Appendix B.1.

## B Numerical Error Estimates

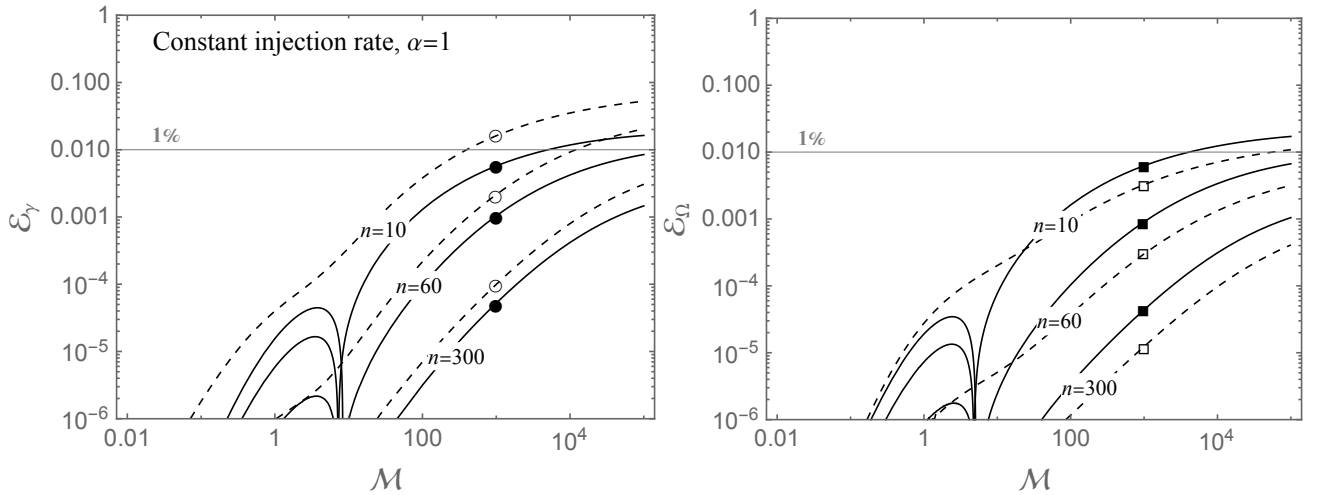


Figure B.1: Method-of-lines error for solutions with various discretization  $n$  in the *constant-injection-rate* case,  $\alpha = t\dot{V}/V = 1$ , as a function of the dimensionless time  $\mathcal{M} = t/t_{MK}(\alpha = 1)$ . **(a)** crack length error relative to  $n = 600$  solution,  $\mathcal{E}_\gamma = |\gamma(\mathcal{M})_n/\gamma(\mathcal{M})_{600} - 1|$ , and **(b)** crack opening at the inlet error  $\mathcal{E}_\Omega = |\Omega(\mathcal{M}, 0)_n/\Omega(\mathcal{M}, 0)_{600} - 1|$ . Solid and dashed lines correspond to the method-of-lines implementations using global (A.2) and local, at the inlet, (A.3) continuity conditions, respectively.

### B.1 Method-of-Lines

The integration of the ODE system (A.4) and (A.5) in the method-of-lines numerical solution (Appendix A) is carried using adaptive-stepping routine in Wolfram Mathematica, and is numerically 'exact' for all practical purposes (i.e. near the machine precision). Method's numerical error is therefore associated solely with the spatial discretization and can be estimated by considering the solution convergence with increasing number  $n$  of the spatial nodes, Figs. B.1-B.3. Figs. B.1 and B.2 show, for two injection scenarios, evolution in 'time'  $\mathcal{M}$  of

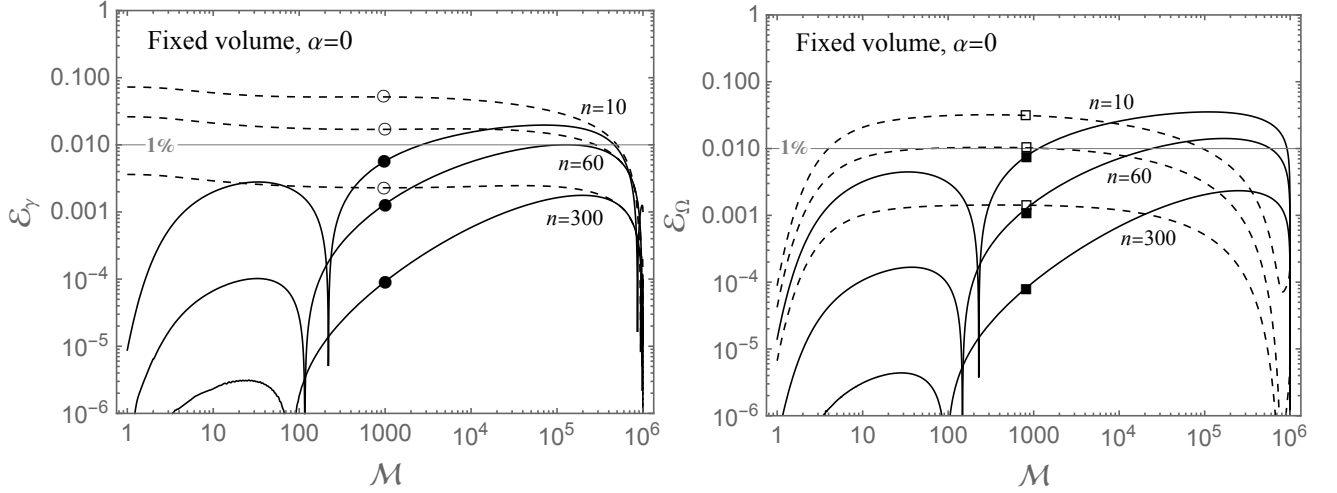


Figure B.2: Same as Fig. B.1 but for the *fixed-volume* injection case  $\alpha = 0$ . The evolution parameter  $\mathcal{M}$  in this case is a dimensionless reciprocal of time,  $\mathcal{M} = t_{MK}(\alpha = 0)/t$ .

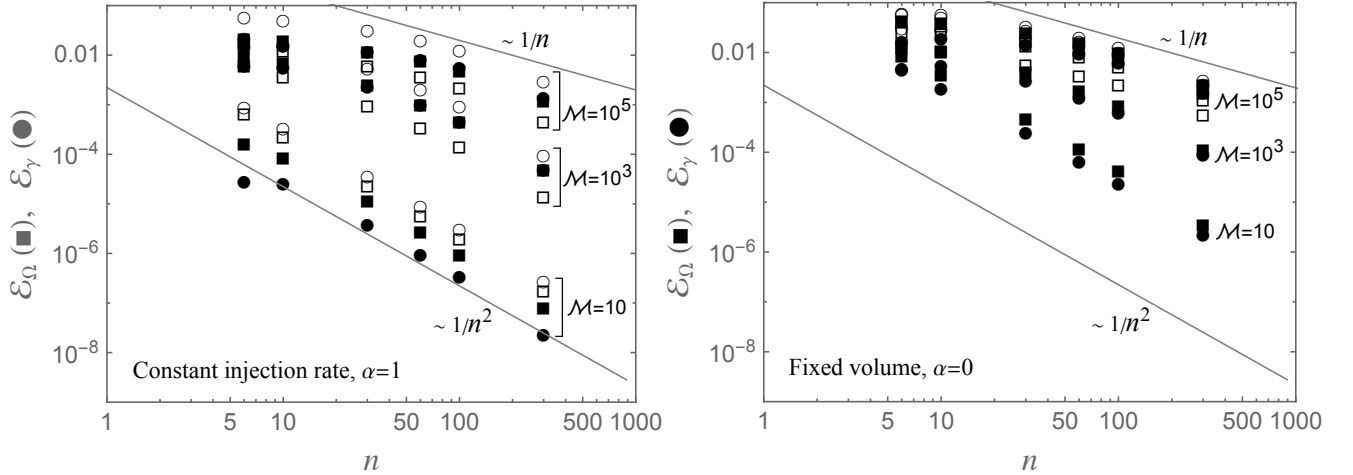


Figure B.3: Convergence of the method-of-lines solution with increasing spatial discretization  $n$  at fixed values of the evolution parameter  $\mathcal{M} = 10, 10^3, 10^5$  in the case of (a) constant injection rate,  $\alpha = 1$ , and (b) fixed volume injection,  $\alpha = 0$ . Solid and empty symbols correspond to the method-of-lines implementations using global (A.2) and inlet (A.3) continuity conditions, respectively. The method utilizing the global continuity, in both constant-rate and fixed-volume cases, converges as  $\sim 1/n^2$  at intermediate values of  $\mathcal{M} = 10, 10^3$ , and slower, as  $\sim 1/n$  in the viscosity-dominated regime  $\mathcal{M} = 10^5$ . On the other hand, the method utilizing the local-inlet continuity has slower  $\sim 1/n$  in the fixed-volume case, (b), in the entire range of  $\mathcal{M}$ .

the errors in crack length and opening value at the inlet for solutions at various discretization  $n$ . in two cases of constant-rate-injection,  $\alpha = 1$ , and fixed-volume,  $\alpha = 0$ , respectively. The error is defined as the relative distance of the solution for a given  $n$  from the one with the largest value of  $n$  considered ( $n = 600$ ). The error of the method with the global continuity implementation (solid lines and solid symbols in the Figures) is seen to increase with  $\mathcal{M}$  towards the viscosity-dominated limit for both constant-rate and fixed-volume injection cases, where this limit is reached at large and small times, respectively. This remains true for the method with the local-inlet continuity implementation (dashed lines and open symbols) for the constant-rate case (Fig. B.1), but the error remains approximately insensitive to the value of  $\mathcal{M}$  in the fixed-volume case (B.2). (Abrupt decrease of the error near the largest value of  $\mathcal{M} = 10^6$  in the fixed-volume solutions is an artifact of the initialization of the solution in this case). Overall, when both injection cases considered, the method based on global continuity is seen to result in lower error compared to the method based on the local-inlet continuity. Fig. B.3, which shows solutions' errors, sampled at few values of  $\mathcal{M}$ , vs. spatial discretization  $n$ , illustrates the convergence of the numerical methods.

## B.2 Equation-of-Motion

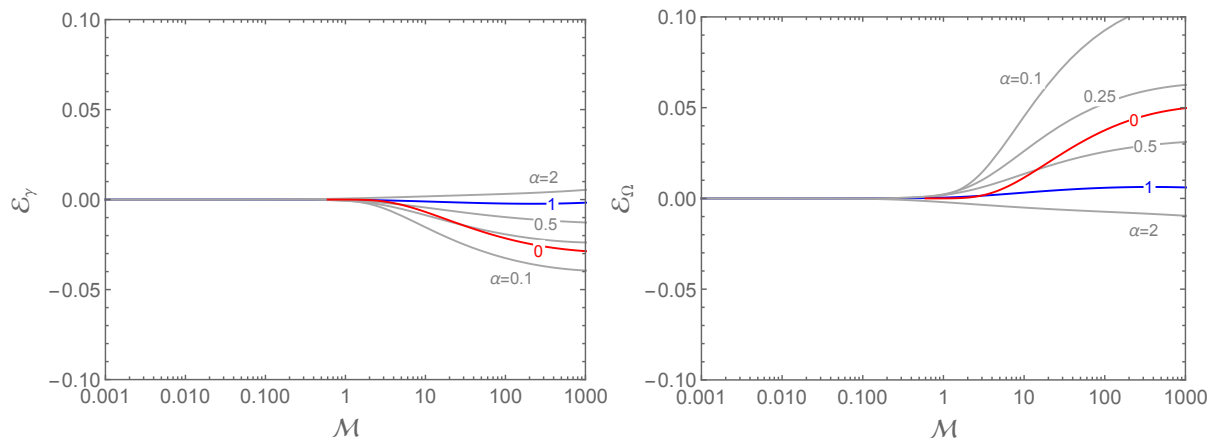


Figure B.4: Relative error of the EofM solutions,  $\mathcal{E}_\gamma = \gamma_{\text{EofM}}/\gamma_{\text{MofL}} - 1$  and  $\mathcal{E}_\Omega = \Omega_{\text{EofM}}(0)/\Omega_{\text{MofL}}(0) - 1$ , for various injection power-laws  $\alpha = t\dot{V}/V$  as function of evolutionary variable  $\mathcal{M} = (t/t_{MK}(\alpha))^{2\alpha-1}$ . Both the EofM and the full numerical, method-of-lines (MofL) solutions with  $n = 50$  are as shown in Fig. 5.

Approximation error of an EofM solution is considered relative to the corresponding fully numerical, method-of-lines solution with  $n = 50$ , and illustrated as a function of dimensionless evolution variable  $\mathcal{M}$  on Fig. B.4 for various injection power-laws  $\alpha$ . Method-of-lines solutions are indeed very accurate (error of solutions with  $n = 50$  is bounded by  $\sim 0.001$  (0.1%) in the considered range of  $\mathcal{M}$ , see Figs. B.1-B.3), and, thus, appropriate to serve as a reference in defining the EofM solution error. It is observed, e.g., that the EofM solution for the case of constant injection rate is very accurate with the error (shown in linear scale) discernible only as solution approaches the viscosity-dominated regime, where it remains sub 1%. The error is seen to increase significantly in the viscosity-affected part of the solution for small

injection power-law values  $\alpha$  (see for example the error for the lowest-non-zero value  $\alpha = 0.1$  shown). Error of the EofM solution for the fixed-volume case,  $\alpha = 0$ , is bounded by 3% for the crack length and 5% for the opening at the inlet. Possibly surprising result that error for  $\alpha = 0$  case is less than for the cases with  $\alpha = 0.1$  and  $\alpha = 0.25$  is understood upon recalling different opening spatiotemporal approximation that has been used in the EofM construction for injection  $\alpha > 0$  (41) and the fixed-volume  $\alpha = 0$  (42) cases. With the former approximation deteriorating with decreasing power-law  $\alpha$ .